A Novel Design Methodology For Enhanced Compressor Performance Based on a Dynamic Stability Metric

by

Juan Carlos Castiella Ruiz de Velasco

B. Ing. Ingeniería Industrial, Universidad de Navarra (2001)

Submitted to the Department of Aeronautics and Astronautics in partial fulfilment of the requirements for the degree of

MASTER OF SCIENCE IN AERONAUTICS AND ASTRONAUTICS

at the

MASSACHUSETTS INSTITUTE OF TECHNOLOGY

[February 2005]

January 2005

Author _____

Department of Aeronautics and Astronautics
January 28, 2005

Certified by _____

Professor Zoltan Spakovszky
C.R. Soderberg Assistant Professor of Aeronautics and Astronautics
Thesis Supervisor

Accepted by _____

Jaime Peraire
Professor of Aeronautics and Astronautics
Chair, Committee on Graduate Students

A Novel Design Methodology For Enhanced Compressor Performance Based on a Dynamic Stability Metric

by
Juan Carlos Castiella Ruiz de Velasco

Submitted to the Department of Aeronautics and Astronautics in January 28, 2005, in partial fulfilment of the requirements for the degree of Master of Science in Aeronautics and Astronautics

Abstract

This thesis introduces a new way to quantify the stability of compression systems. Unlike surge margin, the new metric is directly related to the damping of the natural oscillations of the compression system that lead to rotating stall and surge. Furthermore, the new metric captures the shape of the compressor characteristic such that it accounts for the sensitivity of compressor stability to changes in operating line conditions. This metric is used as a primary design variable in a compressor optimization design framework with the goal to enhance compressor performance and operability. The novel design methodology is applied to a generic three stage axial compressor. The baseline three-stage compressor design is optimized to demonstrate the potential performance and operability improvements. More specifically, the work presented in this thesis addresses the following objectives:

Development of a New Stability Metric Based on Dynamic Considerations. The simulation results indicate that there is no correlation between surge margin and damping of the compression system and that the changes in damping ratio along the operating line much more fundamentally represent the dynamic behavior and stability margin of the compression system. From this a new dynamic stability metric is developed which is comprised of two parts: (1), the dynamic behavior of the compression system at operating conditions is captured by quantifying the growth rate of the perturbations in the flow field, and (2) the shape of the compressor characteristic is accounted for to quantify the deterioration in compressor dynamic stability with changes in working condition.

Implementation of the New Stability Metric in a Compressor Design Optimization Framework. The new compressor design optimization framework allows a versatile definition of the objective function such that any combination of pressure ratio, efficiency and dynamic stability can be prescribed at various operating speeds. The compressor design optimization framework uses an effective blade-to-blade CFD method (fast blade performance prediction method) to predict the blade row performance which is used to evaluate the compressor performance and dynamic stability. The fast blade performance prediction method is estimated to be 100 times faster than a direct numerical simulation and it is shown that the accuracy is within 2% of the direct numerical simulation results.

Design Optimization of a Generic Three Stage Compressor. Two different design philosophies commonly used in compressor design practice are adopted. The first design philosophy is aimed at improving efficiency and the second is targeted to improve operability over the entire compressor operating range.

The compressor design optimization for enhanced efficiency demonstrates that improvements in efficiency are due to an optimal matching of the compressor stages. The results show an average efficiency improvement of 1% throughout the operating envelope. At maximum climb conditions an efficiency enhancement of 2.7% is achieved. Furthermore, optimizing for efficiency does not deteriorate stability but yields an average improvement in surge margin of 2.6 points. The compressor design optimization based on dynamic stability provides on average a 23% improvement in the newly developed stability metric which translates into a surge margin enhancement of 4 points on average across the entire compressor map. Furthermore it is observed that the compressor design optimization for enhanced dynamic stability also results in an improvement in compressor efficiency of 0.65 points throughout the operating envelope.

The outcomes of this thesis are encouraging and it is suggested to apply the developed optimization framework and novel stability metric to an industrial strength problem to assess the capabilities in a real compressor environment.

Thesis Supervisor: Professor Zoltán Spakovszky
Title: C.R. Soderberg Assistant Professor of Aeronautics and Astronautics

Acknowledgments

I first wish to thank Professor Spakovszky for his systematic dedication and for the continuous support and encouragement he has provided throughout my stay at MIT. I am particularly thankful for his constructive critical look at my work and effective counseling leading to a greater learning experience.

I must also thanks my office-mates, Vai-Man, Bobby and Nate for sharing their experience at GTL with me and for the many conversations we had over the last year and a half.

I also would like to thanks my roommates, Vince and John for introducing me to the Canadian way of life and most of all for their friendship that I am sure will endure over the years to come.

Finally, my last thanks go to my family and Andrea, whose unconditional support and visits have been essential to the overall success of my stay at MIT.

Contents

List of Figures

List of Tables

Nomenclature

Acronyms

CFD	Computational Fluid Dynamics
DEB	Disturbance-Energy Balance
DF	Diffusion Factor
GTL	Gas Turbine Laboratory
IC	initial conditions
MG	Moore-Greitzer
MIT	Massachusetts Institute of Technology
NS	Neutral Stability
PR	Pressure Ratio
SM	Surge Margin
SM	Stall Margin
SQP	Sequential Quadratic Programming

Greek

α	absolute flow angle
β	relative flow angle
Δ	difference (when used as a prefix)
δ	deviation angle, perturbation, damping
ξ	damping ratio, weighting factor
ϕ	flow coefficient
γ	stagger angle
χ	unstaggered metal angle
φ	camber angle
η	adiabatic efficiency
λ	blade passage inertia
μ	stator blade-row inertia
ρ	air density
Ω	rotational speed
σ_n	growth rate

ω blade row loss coefficient, frequency

ω_n rotation rate

Ψ pressure rise coefficient

τ unsteady-losse time lag

Roman

a speed of sound

A cross-sectional area

B transmission matrix

c_P specific heat at constant pressure

c blade-row chord, polynomial interpolation coefficients

i index, incidence

j index, $j=\sqrt{-1}$

k_t throttle coefficient

L loss coefficient

m mass

$\dot{m}$ mass flow

M Mach number, number of discrete points along the characteristic

n harmonic number

N rotation speed, number of stages

P pressure

p weighting factor

Q amplification factor

r radius

R mean radius, stage reaction

Re Reynolds number

s eigenvalue, Laplace variable, blade pitch

T temperature

U wheel speed

V non-dimensional velocity

X transmission matrix

Y transmission matrix

Superscripts

$_{TS}$	total-to-static
$\bar{}$	mean quantity
$'$	in relative frame

Subscripts

$_1$	inlet or upstream
$_2$	outlet or downstream
$_{AVE}$	averaged value
$_{corr}$	corrected value
$_{des}$	at design
$_{dist}$	distribution
$_i$	initial
$_{line}$	line
$_{NS}$	at neutral stability
$_{nomr}$	reference value
$_{OP}$	at the operating point
$_\theta$	in tangential direction
$_R$	rotor
$_{speed}$	speed
$_S$	stator
$_{sys}$	system
$_x$	in axial direction
$_T$	stagnation quantity

Chapter 1

Introduction

Compressor design is an ever growing discipline driven by the desire of producing safer, cleaner and cheaper engines. Over the past four decades, aerodynamic research programs have focused on efficiency to reduce operating costs. In the late nineties, Greitzer and Wisler [11] showed that the potential for cost reduction obtained from further improvements in efficiency was low and recommended new research areas with further cost reduction opportunities. Since then, the aero-engine industry has engaged in some of these research areas, mainly related to the affordability and operability of compressors. Current research efforts concentrate on the manufacturing of simpler, fewer parts, and lighter, higher thrust-to-weight engines. Also more recently a new research direction was launched that focuses on the improvement of the robustness of the design to manufacturing variabilities, noise reduction and operation free from instabilities (Garzon [10], Lamb [15], Sidwell [22]).

In order to ensure the safe and stable functioning of the engines throughout the operating envelope the compressor design must be robust to inlet distortion, compressor deterioration, foreign object ingestion and acceleration transients. In order to satisfy the design requirements set by the customer the compressor design is achieved iteratively with the goal to meet stability, pressure ratio and efficiency targets across the compressor map. Each iteration is composed of two design phases. The first phase uses vector diagram design to determine the compressor annulus shape and the radial distribution of velocity and flow angles along the compressor. The second phase defines the blade profiles necessary to achieve the desired velocity and pressure distributions. Upon completion of the two design phases, the performance, pressure ratio and stability of the compressor are evaluated. While maximum values of efficiency and pressure

ratio are desired a minimum amount of stability margin must be met. Generally, changes to the initial compressor architecture are necessary and the iterative process is conducted until the final optimal compressor design is obtained (Smith [24]).

Currently the stability of the compressor is measured using a steady-state stability metric known as surge margin. Surge margin does not assess the dynamic state of the compression system limiting its performance. This thesis proposes a new stability metric, S_D, based on the dynamic behavior of the compression system. S_D, as opposed to surge margin, captures the dynamic state of the flow field inside the compressor at operating conditions and the deterioration of dynamic stability with changes in operating conditions. The knowledge of the dynamic behavior of the compression system captured in S_D is suggested to be used to achieve more aggressive compressor designs and to obtain improvements in performance while guaranteeing the required levels of operability. The potential for performance improvement can be maximized if S_D is introduced as a prime design variable in the iterative compressor design optimization. The outcome of such methodology could yield compressor designs with enhanced efficiency, pressure ratio and operability.

1.1 Technical Background

Gas turbines produce shaft power or thrust over a range of operating speeds. Ensuring that this occurs demands a certain pressure rise and efficiency from the compressor to fulfill the turbine demands and complete the thermodynamic cycle. Further, gas turbines must be able to run free of instabilities over the entire operating envelope. While pressure ratio and efficiency can be estimated relatively accurately during the preliminary design phase, the prediction of instability remains a challenge and thus has been the focus of much research in the past.

1.1.1 Compressor Stability

Compression systems present two major types of large scale instabilities, surge and rotating stall. Surge is an engine wide phenomenon where the annulus averaged mass flow oscillates with time (3-10Hz) as illustrated in Figure 1-1 on the left. On the other hand, during rotating stall the annulus averaged mass flow remains more or less

constant but the local mass flow varies with time as rotating wave structures travel in the circumferential direction (20-50Hz) as shown in Figure 1-1 on the right. Investigating the inception mechanisms of these instabilities is important because surge and rotating stall limit the performance and the stable range of the compressor.

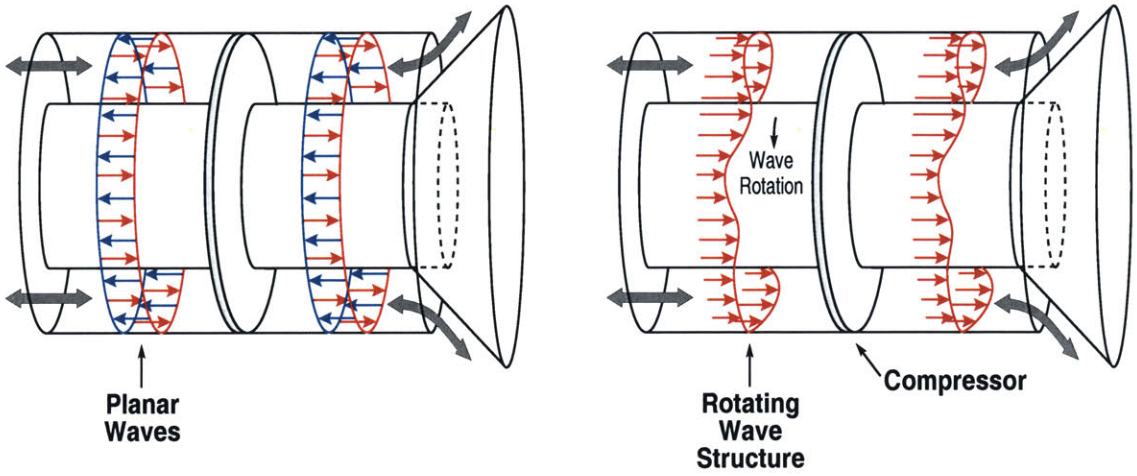

Figure 1-1. Two types of compressor instability phenomena: surge (left) and rotating stall (right).

1.1.1.1 Static stability

There are two criteria to assess the stability of a compressor. The first criterion refers to static stability and is formulated in [13]: Static stability requires that the slope of the throttle line be always larger than the slope of the compressor characteristic.

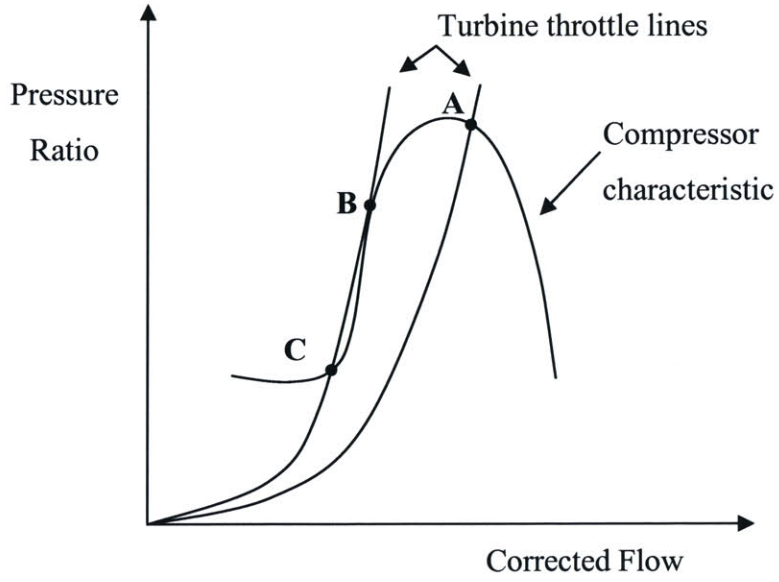

Figure 1-2.Static Stability- Statically unstable operating point B.

Figure 1-2 illustrates the static stability criterion. Suppose that the compressor is operating at point A. A sudden deficit in compressor mass flow will yield a higher pressure rise than that demanded by the turbine. This will accelerate the flow and return the operating point back to the original point A. If the same sudden mass flow change occurs at point B, the turbine will demand a higher pressure rise from the compressor than it can provide. The result is a statically unstable compressor which is associated with a pure divergence from the initial state B.

1.1.1.2 Dynamic stability

The static stability criterion does not capture the dynamic flow phenomena taking place inside the compressor and thus is not a sufficient criterion to avoid instability (Greitzer [13]). The observed instability phenomena in practice are characterized by a growing oscillatory motion about an initial operating point manifesting the dynamic nature of these instabilities. If these small amplitude perturbations of the flow field continue to grow with time, one of the two types of large scale instabilities, surge and rotating stall, will appear.

Rotating stall appears as a circumferentially non-uniform flow distribution around the annulus at 20-70% of the rotor speed. McDougall et al. [18] and Day [6] identified two different inception mechanisms for rotating stall. So called "spikes" are sudden short length scale disturbances (of the order of one blade pitch) which provoke flow breakdown causing the compressor stall. The second path into instability, referred to as modal stall inception (Moore and Greitzer [19]), involves the temporal growth of larger length scale circumferential perturbations (of the order of the compressor circumference). As mass flow is decreased rotating stall will be initiated in the form of spikes if the critical incidence of any of the stages in the compressor is exceeded before reaching the top of the total to static pressure rise characteristic. Otherwise, flow breakdown can be initiated by modal stall (Camp and Day [4]).

Surge is an engine wide phenomenon. This large scale instability appears in the form of circumferentially uniform waves oscillating in the longitudinal direction at low frequency (5% of rotor speed).

This thesis focuses on rotating stall in high-speed axial compressors. The compressors investigated have relatively high flow coefficients and low loading such that rotating stall is more likely to be initiated by modal waves. Furthermore the hub-to-tip radius ratios are high and the incidence into the individual blade rows are such that the peak of the pressure rise characteristic is reached before the critical incidence is exceeded (Camp and Day [4]).

1.1.2 Previous Work

Already in the early days of compressor development, achieving sufficient levels of stability throughout the compressor map was one of the main concerns and challenges in compressor design. In the early fifties, Lieblein et al. [16] introduced the diffusion factor. This parameter allows to assess the blade loading near stall. However, the diffusion factor is not suitable to explain the mechanisms leading to rotating stall and surge. Up until the eighties, sufficient levels of stability were ensured using stall prediction methods mostly based on experience and correlations (Smith [24]). Over the past two decades, the introduction of CFD and a better theoretical understanding of the processes leading to stall and surge has enabled improved compressor designs with enhanced operability. In particular, the work by McDougall [18] and Day [6] identifies two inception mechanisms of stall, "spike" and "modal oscillations". Moore and Greitzer [19] report a theory to predict the modal stall inception of rotating stall. They are able to trace the evolution of disturbances in the compressor system and identify the top of the non-dimensional total-to-static pressure rise characteristic as the limit of stable compressor operation. Moreover, they show that pure surge and rotating stall modes can exist without one another but are coupled in general. Longley [17], reviews the Moore-Greitzer based dynamic compressor modeling and discusses the importance of further research necessary in the modeling of three-dimensional flow phenomena. Bonnaure [2], Feulner [8] and Weigl [27] introduce compressibility considerations into the existing Moore-Greitzer models and Frechette [9] uses the newly gained understanding of the compressible dynamic stability phenomena to introduce the concept of disturbance energy. He also suggests that in the compressor design phase a potential for performance improvement exists if dynamic stability replaces surge

margin. This idea opens the door to new design possibilities and constitutes the basis on which this thesis is built. Dorca [7] further develops the work done by Frechette and uses the dynamic compressor model developed by Spakovszky [25] and basic dynamic system modeling to establish a new set of stability metrics. In addition, Dorca establishes a relation between stable flow range and dynamic stability, referred to as the Equivalent Curvature Relation. This tool proves to be useful during preliminary compressor design and helps to establish a first approximation to the compressor characteristic with the desired dynamic stability, pressure ratio and mass flow.

The stability metrics proposed by Dorca [7] seem to be limited for application to industrial compressor design and are discussed in Chapter 2. Particularly, the disturbance energy approach is computationally expensive and the equivalent curvature relation does not account for general variations in shape of the compressor characteristic.

More recently, Perrot [22] reports the implementation of a compressor design optimization framework using surge margin as the prime design variable. He demonstrates a 6% improvement in surge margin of a 3 stage compressor at design conditions at the cost of a 0.5% drop in efficiency and a 2% decrease in pressure ratio.

The research in this thesis builds on the work by Frechette [9], Dorca [7], and Perrot [22] and addresses their shortcomings by introducing a new stability metric based on dynamic considerations coupled with a compressor design optimization framework.

1.1.2.1 Current stability metrics

Ideally, one would like to obtain the maximum possible compressor efficiency and pressure ratio. In practice however, the operating points must be kept at a "safe" distance from the limit of stable compressor operation. This limit is referred to as the surge line. A certain amount of surge margin must be guaranteed (usually about 20-30%) to ensure that the operating condition will remain in the stable operating region throughout the operating envelope and in the presence of inlet flow distortion, engine deterioration or acceleration transients.

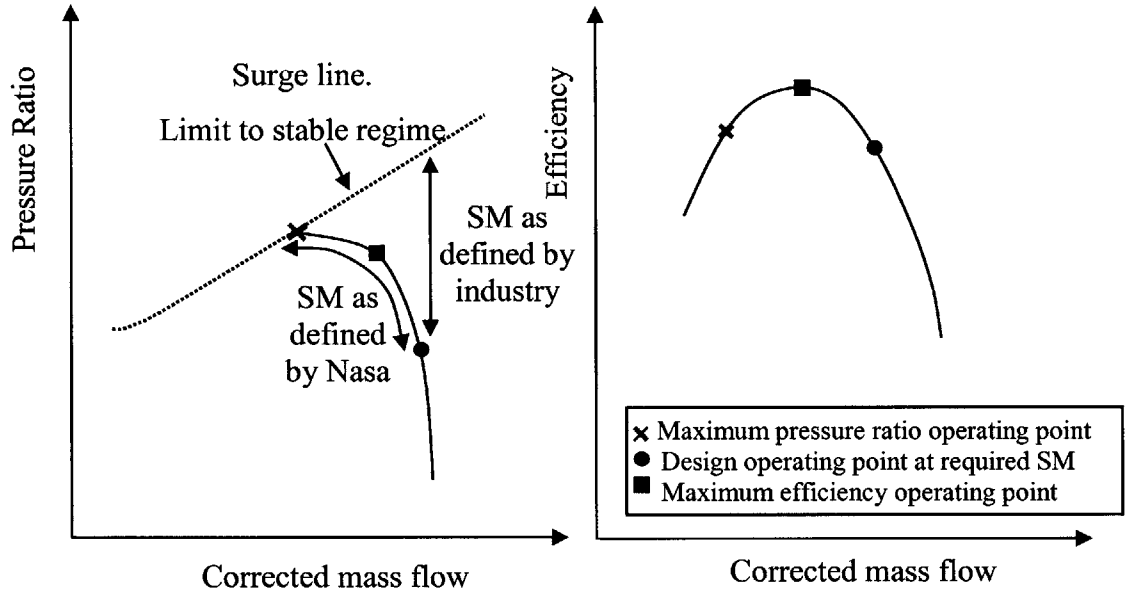

Figure 1-3. Compressor and efficiency maps illustrating the definition of surge margin

The amount of surge margin or distance between the operating point and the surge point in the compressor map is commonly quantified using two different definitions. Figure 1-3 illustrates both definitions of surge margin. Surge margin as commonly defined in industry evaluates the distance between the operating point and the surge point at constant corrected mass flow. On the other hand, surge margin as defined by NASA measures the distance between the operating point and the surge point at constant corrected speed. The NASA definition of surge margin accounts for throttle area changes representing the equivalent throttling process required to take the compressor into stall (Cumpsty [5]). Figure 1-3 also illustrates that the demands in surge margin limit the maximum possible compressor performance in pressure ratio and efficiency. It is evident from the schematic that operating points of maximum pressure ratio, maximum efficiency and minimum surge margin do not coincide. Thus performance must sometimes be compromised with operability in the compressor design.

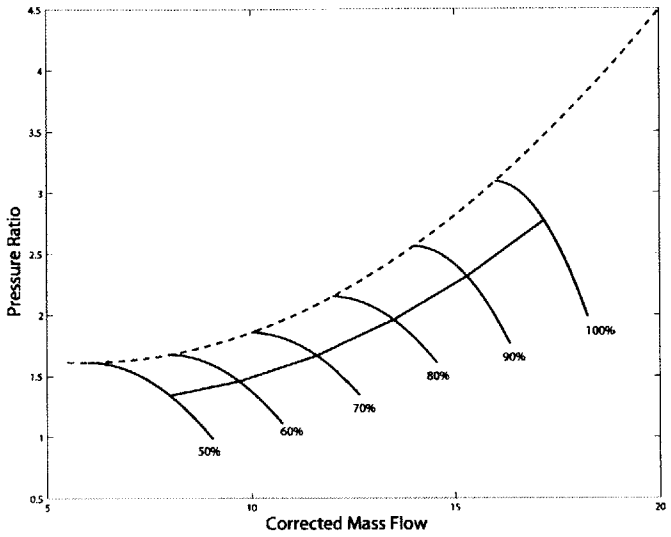

Figure 1-4. Compressor map for a generic compressor with $SM_{Industry}$=25% throughout the operating envelope.

Figure 1-4 illustrates the compressor map for a generic 3 stage compressor with an operating line fixed such that the surge margin as defined in industry is 25% throughout the operating envelope. In order to assess if the two definitions of surge margin represent the same operability trends their values are calculated across the operating envelope.

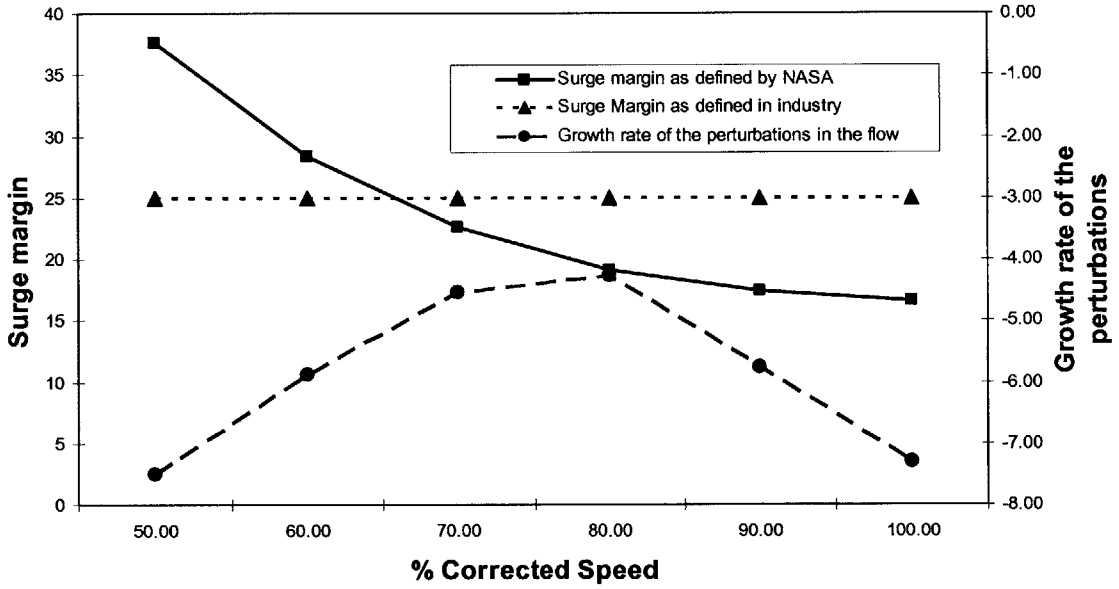

Figure 1-5. Surge margin as defined by NASA and industry and growth rates of the perturbations in the flow field for the operating points defined in Figure 1-4.

Figure 1-5 presents the values of the two surge margin definitions at the operating conditions illustrated in Figure 1-4. Clearly, the two definitions do not represent the same levels of surge margin since as the value of surge margin as defined by NASA decreases with increasing speed, the value of surge margin by the industry definition remains constant. As outlined earlier, the dynamics of the compression system dominate the compressor stability behavior. A detailed analysis of the dynamics of the same compression system was conducted using the modeling methodology outlined later in this thesis. The goal was to identify if any of the two definitions of surge margin captured the dynamic phenomena taking place in the compressor flow field. The results show that neither of the two definitions of surge margin capture the dynamics of the compression system, represented here by the growth rate of the small amplitude perturbations in the flow field. The limitations to capture the dynamic stability of the compressor of both definitions of surge margin suggest an opportunity for a new stability metric based on dynamic considerations. Furthermore, the incorporation of such a metric in the compressor design phase is conjectured to enable more aggressive compressor designs enabling improvements in performance while insuring adequate levels of stability. This thesis is based on existing compressor stability models (Spakovszky [25]) that have enabled a description of the stability phenomena and are used to evaluate the new stability metric. The new stability metric is then used in a compressor design optimization framework to enhance performance and stability.

1.1.3 Off-Design Performance of Multi-Stage Compressors

Fixed geometry compressors (i.e. low pressure compressors without variable stator vanes) are designed such that the compressor efficiency is maximized where the engine operates most of the time, that is generally at the design point (Cumpsty [5]). However, engines do also operate at off-design conditions which still demand adequate levels of pressure ratio, efficiency and stability. The operability requirements across the compressor map might not be achievable with a fixed geometry such that compromises need to be made, usually with emphasis on stability at low speed and efficiency at design conditions (Cumpsty [5]).

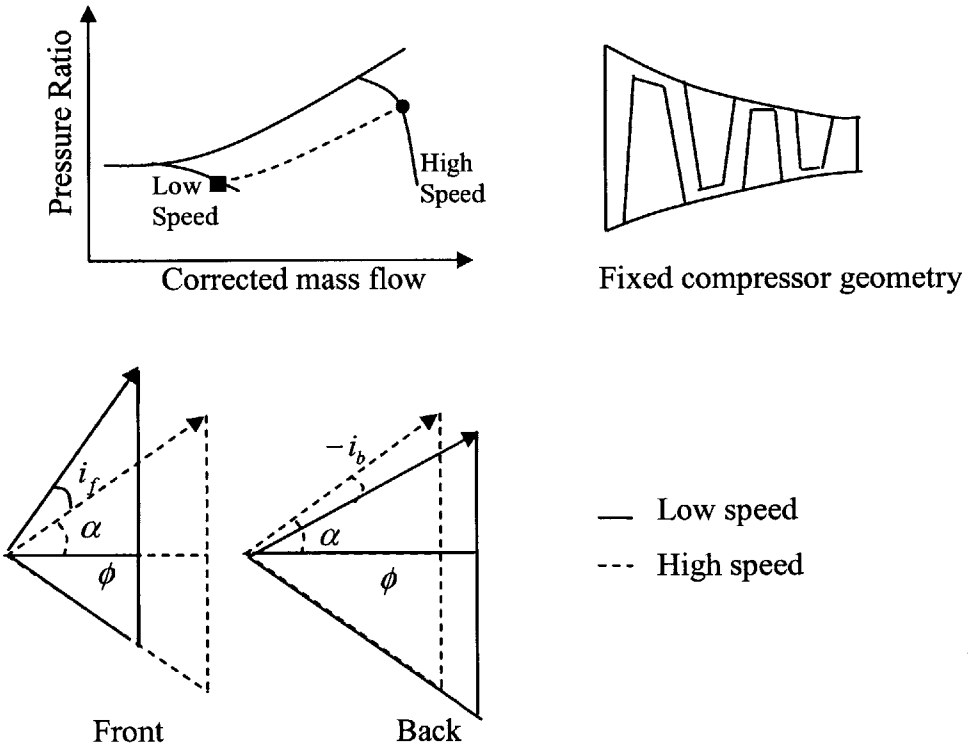

Figure 1-6. Compressor map, gas flow path and non-dimensional velocity triangles of a generic compressor.

To illustrate the effects of off-design performance and stage matching on blade row performance consider the following example. The flow coefficient $\phi=V_x/U$ determines the incidence and thus, if Mach number effects are ignored, the performance of the individual blade rows. As operating conditions change, the flow coefficients into the individual blade rows will depart from their nominal values. This causes some of the stages to choke and others to stall. This occurrence is illustrated in Figure 1-6 which shows schematically two speed lines and the corresponding operating points together with the gas path flow area along the compressor. The pressure rise along the machine, which is larger at high speeds than at low speeds, leads to an increased density rise at high speed operation compared to the low speed operation. The fixed gas path contraction is chosen to achieve the required flow coefficients at design conditions.

Figure 1-6 shows the velocity triangles at the front and the back of the compressor for low and high speed operation. The velocity triangles at design speed are the same for the front and the back stages ($\phi_{Design\ front} = \phi_{Design\ back}$) since the area contraction was designed to accommodate the changes in density along the compressor

at design speed. At off-design conditions (lower speed) the density rise along the compressor is reduced while the gas flow path area is unaltered. The result is an increase in incidence at the front of the compressor, i_f (due to the lower flow coefficient), and a decrease in incidence at the back of the compressor, i_b (due to the higher flow coefficient). This is a common trend in axial compressors when the operating speed is reduced from design conditions: the front stages are closer to stall (lower flow coefficient) and the back stages are closer to choking (higher flow coefficient). In the design of fixed geometry compressors, one must decide on the admissible variation in operating conditions to satisfy the requirements in pressure ratio, efficiency and stability across the compressor map.

In order to match the stages over the operating range, multi-stage compressor designs often include variable stator vanes and bleed valves. Such concepts enable to meet the required performance at design and off-design operating conditions but generally increase the complexity and weight of the compression system. The compressor design optimization framework introduced in this thesis offers a new approach to compressor matching without the use of variable geometry or air bleeds. This could potentially reduce the weight and complexity of the compressor architecture.

1.2 Conceptual Approach

This thesis proposes a new stability metric denoted S_D that captures the dynamic state of the compression system at design and off-design operating conditions. S_D evaluates the growth rates of the perturbations in the flow field, which as reported by Moore and Greitzer [19], are directly linked to the slope of the non-dimensional total-to-static characteristic. Additionally, S_D assesses the robustness of the compression system stability to changes in operating conditions. This quantity captures the shape of the non-dimensional total-to-static pressure rise characteristic. The description and quantification of the dynamic behavior of the compression system using S_D is suggested to enable potentially more aggressive compressor designs and improvements in compressor performance while guaranteeing the required dynamic stability of the compressor over the entire operating envelope.

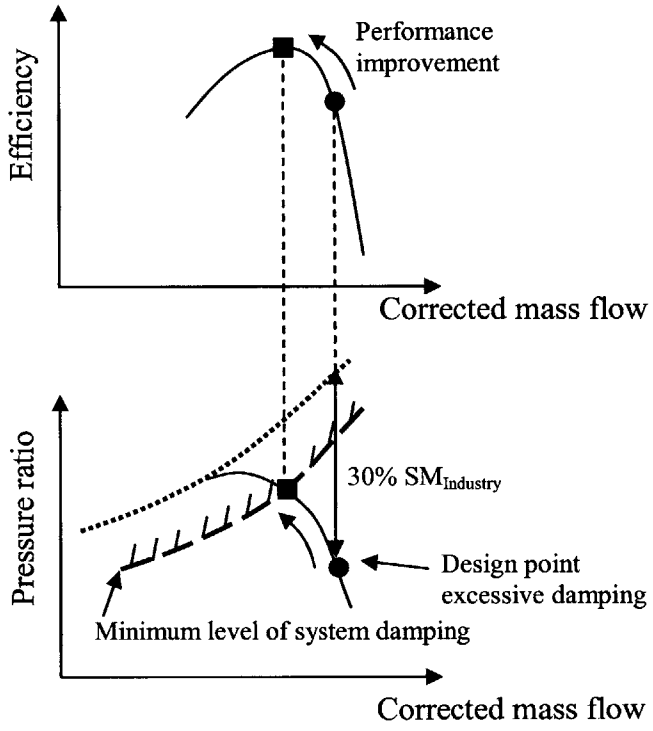

Figure 1-7. Potential for performance improvement while maintaining the required level of system damping

Figure 1-7 illustrates the potential for performance improvement using the novel stability metric. Since dynamic stability and surge margin do not correlate (Figure 1-5), the dynamic compression system might be overdamped when operating at the required surge margin. This excess in dynamic stability provides an opportunity to open the design space to more aggressive designs and to obtain improvements in compressor performance. Figure 1-7 shows the new operating point if the minimum level of system damping is used instead of surge margin with a substantial improvement in compressor performance.

To assess the potential improvement in performance using the new stability metric, a compressor design optimization framework is developed. The key feature of this methodology is that stability, quantified using the new metric based on the dynamic behavior S_D, is used as one of the prime design variables. In the design optimization each blade profile geometry is varied affecting the blade loss characteristics and hence the overall compressor performance and stability. A set of constraints and an objective function are evaluated and checked until the process converges. In more detail the

optimization framework consists of the following steps and procedures. First, the compressor performance and dynamic stability are computed and evaluated using a mean-line flow solver, dynamic compressor stability models and a blade-to-blade CFD analysis. Then, the results are compared to the desired objectives. If the objectives and constraints are met the optimization will end, otherwise the geometry will be further modified until the requirements in compressor performance and dynamic stability are fulfilled.

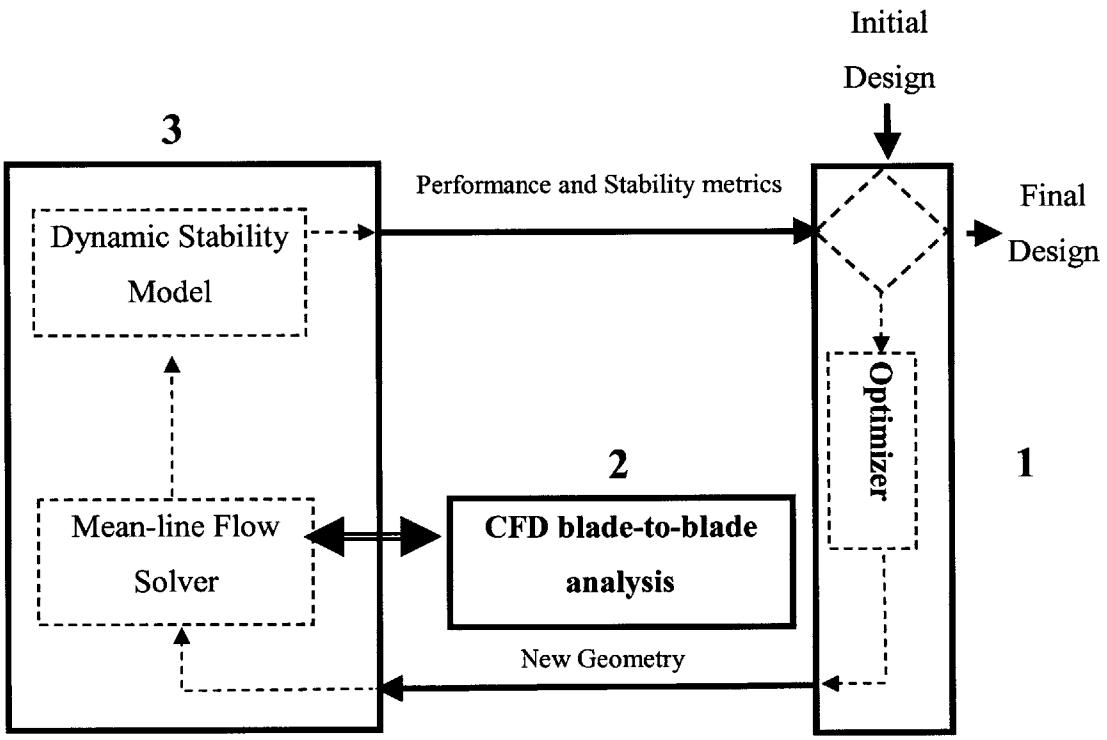

Figure 1-8.Optimization Framework.

Figure 1-8 presents the different modules of the compressor design optimization framework. The optimizer module (1) compares the compressor performance and stability with the user defined objectives and constraints and decides on the changes necessary in the compressor geometry to obtain an improved compressor design. The simulation module (3) includes a mean-line flow solver and a dynamic stability model. The mean-line flow solver is a 1-D compressible flow analysis for multi-stage compressors providing the performance of the compressor geometry and the time averaged flow field quantities necessary for the dynamic stability calculation. The dynamic model uses the uniform flow field quantities provided by the mean-line flow

solver and the slopes of the loss buckets provided by the CFD blade-to-blade analysis (2) to provide the dynamic stability information necessary to determine the new stability metric S_D. In this thesis, the compressor design optimization framework is applied to a generic 3 stage compressor with the goal to redesign the machine for maximum efficiency at high operating speeds and for maximum stability both at high speed and at near idle speed.

1.3 Thesis Organization

This thesis is organized as follows. In Chapter 2, the new dynamic stability metric is derived and its potential for performance and operability improvements is discussed. Chapter 3 focuses on general geometric blade design considerations and on the developments of the fast blade performance prediction module. The details of the optimization framework are described in Chapter 4. Various optimizations strategies for maximum performance and stability of a generic 3 stage compressor are presented and the results and potential impact of the approach are assessed. Finally, Chapter 5 summarizes the findings and results and discusses future work to be pursued.

1.4 Thesis Objectives

The objectives of this thesis are to:

- Assess the shortcomings of surge margin and make the case for a new set of dynamic stability metrics.
- Develop a new set of stability metrics based on dynamic considerations using Spakosvzky's dynamic model [25] and Dorca's [7] metrics for dynamic stability.
- Demonstrate the potential for performance improvement using the newly developed stability metric.
- Set up a compressor design optimization framework and conduct case studies on a three stage generic compressor involving different design philosophies. This will require the following:
    - Create a simple and flexible representation of a family of blades and quantify the effects on performance caused by changes in blade geometry.

- Using blade-to-blade CFD simulations establish an effective link between blade profile geometry, incidence, Mach number and blade performance.
- Implement the new set of stability metrics and the blade performance prediction method in a flexible compressor design optimization framework.

- Demonstrate the potential performance and operability improvements of a 3 stage compressor using the novel compressor design optimization framework.

Chapter 2

Development of a New Stability Metric Based on Dynamic Considerations

This chapter briefly introduces the existing dynamic compressor model [25] used throughout this thesis to predict compressor stability. In addition, previous efforts to develop stability metrics based on dynamic considerations (Dorca [7]) are reviewed. Then the advantages of dynamic stability compared to surge margin are assessed using a generic compressor example. Next the potential performance improvements enabled by dynamic stability considerations are demonstrated. Finally the new stability metric based on dynamic considerations is defined and the benefits compared to conventional stability metrics are assessed.

2.1 Rotating Stall Inception Prediction Model

The objective of the dynamic compressor model is to quantify the temporal evolution of the small perturbations in the flow field to predict the inception of the larger amplitude non-linear phenomena surge and rotating stall. The Moore-Greitzer [19] theory establishes that the grow rates of the perturbations in the flow field vary with the slope of the non-dimensional total-to-static characteristic as follows:

$$\sigma = \frac{\frac{\partial \psi_{ts}}{\partial \phi}}{\frac{2}{|n|} + \mu} \quad \text{where } n \text{ is the harmonic number and } \mu \text{ is the total blade row inertia and} \tag{2.1}$$

$$\mu = \sum_{\substack{\text{Number of} \\ \text{blade rows}}} \frac{c_x}{r \cos^2 \gamma} \text{ is the total blade row inertia} \tag{2.2}$$

Consequently, the Moore-Greitzer theory predicts that the compressor becomes unstable at the top of the non-dimensional total-to-static pressure rise characteristic (σ=0 indicates neutral stability) and that the growth rates of the perturbations in the flow field diminish as the slope of the pressure rise characteristic decreases.

The model used in this thesis is based on an existing modular formulation of the problem capable of dealing with axial and centrifugal compression systems, rotor-stator blade row component interactions and unsteady radially swirling flows (Spakovszky [25]).

In the dynamic modeling approach the following assumptions are made:

- Small perturbations are assumed (linearized problem).
- Compressibility and Reynolds number effects are ignored.
- The flow filed in the inlet and outlet ducts and blade-row gaps is inviscid.
- The hub-to-tip radius ratios in the compressor components are high enough to assume 2 dimensional flow.
- The blade rows are modeled as semi-actuator disks with unsteady blade passage fluid inertia effects and unsteady loss terms.
- Blade-row deviation effects are ignored.
- The background flow field is assumed to be uniform such that the fundamental flow perturbations can be decoupled and hence the flow field can be treated on a spatial harmonic by harmonic basis.

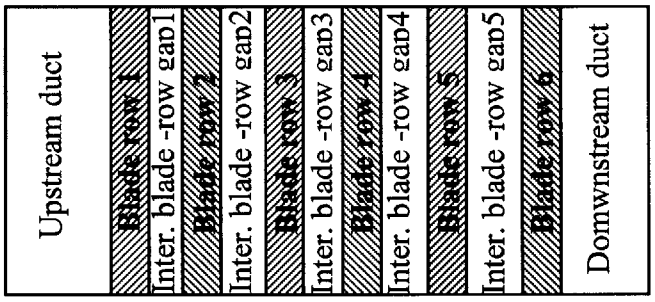

Figure 2-1. Modular design compressor model framework (3-stage compressor example)

In the modular formulation [24], the compressor is modeled as a series of components as shown in figure 2-1. Next, the governing equations for the unsteady flow

field through each duct or inter blade-row gap and rotor or stator blade row are linearized in order to solve for the perturbations in pressure, tangential and axial velocity. The flow field perturbations are written in matrix form in order to obtain the so called transmission matrices for each of the compression system components (for a detailed derivation see Spakovszky [25] and Appendix A):

- n-th harmonic transmission matrix for an axial duct:

$$T_{n,ax} = \begin{bmatrix} e^{nx} & e^{-nx} & e^{-\left(\frac{s}{\overline{V}_x}+jn\frac{\overline{V}_\theta}{\overline{V}_x}\right)x} \\ je^{nx} & -je^{-nx} & \left(-\frac{sj}{\overline{V}_x n}+\frac{\overline{V}_\theta}{\overline{V}_x}\right)e^{-\left(\frac{s}{\overline{V}_x}+jn\frac{\overline{V}_\theta}{\overline{V}_x}\right)x} \\ \left(-\frac{s}{n}-\overline{V}_x-j\overline{V}_\theta\right)e^{nx} & \left(\frac{s}{n}-\overline{V}_x+j\overline{V}_\theta\right)e^{-nx} & 0 \end{bmatrix} e^{jn\theta} \quad (2.3)$$

- n-th harmonic transmission matrix for a rotor blade row:

$$B_{Rot,n} = \begin{bmatrix} 1 & 0 & 0 \\ \tan\beta_2 & 0 & 0 \\ \left[\tan\beta_2 - \tan\alpha_1 - \lambda_{rot}(s+jn) - \overline{V}_{\theta 2}\tan\beta_2\right] & \overline{V}_{\theta 1} - \frac{\partial L_R^{ss}}{\partial V_{\theta 1}}\frac{1}{(1+\tau_R(s+jn))} & 1 \\ -\frac{\partial L_R^{ss}}{\partial V_{x1}}\frac{1}{(1+\tau_R(s+jn))} & & \end{bmatrix} e^{jn\theta} \quad (2.4)$$

- n-th harmonic transmission matrix for a stator blade row:

$$B_{Sta,n} = \begin{bmatrix} 1 & 0 & 0 \\ \tan\alpha_2 & 0 & 0 \\ \left[-\lambda_{sta}s - \overline{V}_{\theta 2}\tan\beta_2 - \frac{\partial L_S^{ss}}{\partial V_{x1}}\frac{1}{(1+\tau_S s)}\right] & \overline{V}_{\theta 1} - \frac{\partial L_S^{ss}}{\partial V_{\theta 1}}\frac{1}{(1+\tau_S S)} & 1 \end{bmatrix} e^{jn\theta} \quad (2.5)$$

Equations (2.3), (2.4) and (2.5) indicate that the uniform background flow field quantities are required to calculate the perturbations in the blade rows, ducts and inter blade-row gaps. Additionally, the sensitivities of the stagnation pressure loss with

respect to the non-dimensional axial and tangential velocities, $\frac{\partial L}{\partial V_x}$ and $\frac{\partial L}{\partial V_\theta}$ need to be calculated in each blade row. As will be demonstrated in Chapter 4, these loss sensitivities are critical for the overall system stability. The transmission matrices contain the dynamics of each of the compression system components and can be stacked together by linking the downstream flow perturbations of one component to the upstream flow perturbations of the following component. This yields a system wide transmission matrix which contains the n-th harmonic dynamic information of the compressor and is in general of the form:

$$X_{sys,n} = T_{ax,n}\left(x_{2\,Nstages+1,1}, s\right)^{-1} \cdot \prod_{i=2\,Nstages}^{i=2} \left[B_{sta,i,n} \cdot B_{gap,2i,n} \cdot B_{rot,i,n} \cdot B_{gap,2i-1,n}\right] \cdot \cdot B_{sta,1,n} \cdot B_{gap,2,n} \cdot B_{rot,1,n} \cdot T_{ax,n}\left(x_{1,N\,\mathrm{int}}, s\right) \tag{2.6}$$

with $s_n=\sigma_n$-jω_n such that σ_n and ω_n are the growth rate and the rotation rate of the n-th harmonic flow field perturbations.

Specification of the inlet and exit boundary conditions of the overall compression system at the end of the upstream and downstream ducts leads to the following eigenvalue problem:

$$\det\begin{bmatrix} EC \cdot X_{sys} \\ IC \end{bmatrix} = 0, EC = [1 \quad 0 \quad 0], IC = \begin{bmatrix} 0 & 1 & 0 \\ 0 & 0 & 1 \end{bmatrix} \rightarrow s = \sigma_n - j\omega_n \tag{2.7}$$

The solution of the eigenvalue problem yields eigenvalues of the form $s=\sigma_n$-jω_n that are used to assess the compression system dynamic stability as will be discussed in next sections.

2.2 Previous Dynamic Stability Considerations

The physical understanding of the rotating stall and surge inception mechanisms has been successfully used for active rotating stall and surge control purposes under the MIT Smart Engine program (Paduano et al. [20]). Beyond the active control applications, Frechette [9] introduces a dynamic stability analysis based on an energy-like quantity, the disturbance energy balance (DEB). DEB quantifies the temporal behavior of the energy of the small perturbations in the flow field. A negative value of DEB is desired since it indicates that the energy of the perturbations in the flow field is

decreasing with time. In addition, Frechette suggests design guidelines to improve operability based on dynamic stability and energy considerations. He concludes that the strongest impact on stability occurs if the geometry of the front stages of the compressor is adjusted. Frechette indicates that the changes required at the front of the compressor to improve operability must increase the loss and deviation of the airfoil profiles, i.e. by increasing stagger angle and camber angle, or reducing blockage, i.e. modify 3D features, and end wall effects. Further, Frechette introduces the concept of blade row powers. Blade row powers measure the contribution in disturbance energy of the individual blade rows to the overall compressor disturbance energy. A negative blade row power indicates that the particular blade row is dissipating the disturbance energy of the compression system and thus is improving the stability of the compression system. A positive blade row power implies that the blade row adds energy to the system.

Dorca [7] uses Frechette's energy concepts to develop a new design tool, the Equivalent Curvature Relation (ECR). ECR establishes a relationship between the flow range from operating point to surge point, the growth rate of the small perturbations in the flow field at operating conditions and the sensitivity of these growth rates to changes in flow coefficient at surge.

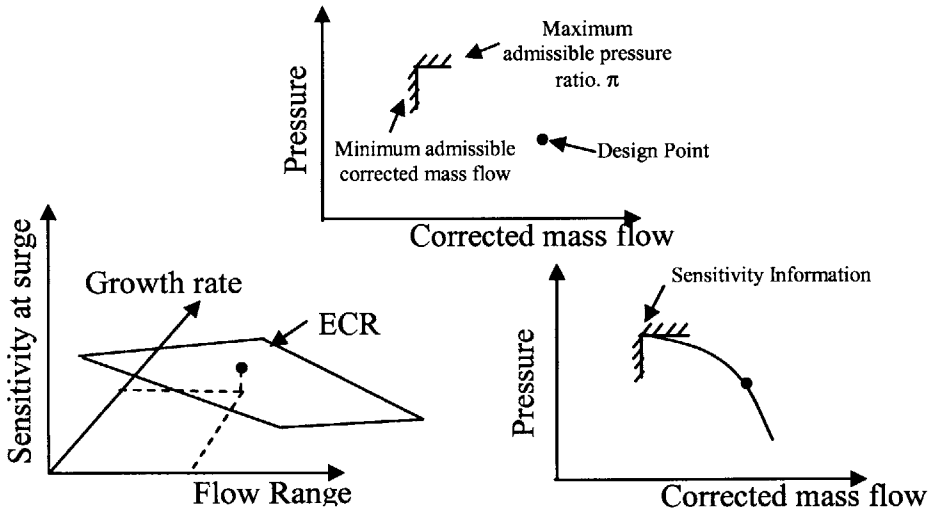

Figure 2-2. Equivalent curvature relationship and related preliminary design methodology

ECR suggests an efficient way of achieving a first approximation to the compressor characteristic during the preliminary design phase. The objective is to

obtain a compressor characteristic that satisfies the demands in pressure ratio, mass flow and dynamic stability at design operating conditions and achieves given maximum pressure ratio and minimum corrected mass flow requirements. These requirements alone are not enough to obtain a first approximation to the compressor characteristic as illustrated in Figure 2-2 (top). However, since the flow range between working points and surge limit and the value of the growth rate of the perturbations are known, ECR provides the value of the sensitivity of the growth rates of the perturbations to changes in flow coefficient (see bottom-left figure in Figure 2-2). The sensitivity of the growth rates of the perturbations to changes in flow coefficient is directly linked to the curvature of the compressor characteristic. This extra information is used with the initial requirements to obtain the first approximation to the compressor characteristic. Then, the iterative optimization process can be initiated with a preliminary compressor design that satisfies the desired dynamic stability and verifying the main requirements in pressure ratio and corrected mass flow.

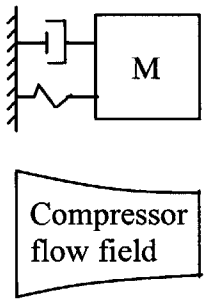

$$x \propto e^{(-\delta + i\sqrt{\omega_n^2 - \delta^2})t} \rightarrow D = \frac{1}{2\xi\sqrt{1-\xi^2}}$$

$$\delta v \propto e^{(\sigma - i\omega)t} \rightarrow Q = -\left(\frac{1}{2\left(\sigma/\omega\right)} + \frac{\sigma/\omega}{2} \right)$$

Figure 2-3. Analogy between compressor dynamics and 1D mass-spring-damper-oscillator

In addition, Dorca discusses a new set of stability metrics based on an analogy between the response of a 1D damped oscillator and the compressor dynamics as scheduled on figure 2-3. The concept of amplification factor Q defined as the ratio of resonant to static disturbance amplitude is introduced to provide a physically meaningful metric. Q=1 means no resonant amplification exists so for example a Q of 1.1 indicates an increase in 10% of the magnitude of the perturbations in the flow field due to dynamic effects. While the conceptual approach is valid, a quantitative analysis of Q shows that in a typical compressor application resonant amplification of the perturbations occurs only for low values of surge margin (SM<5%). For example, for a

rotation rate of ω=0.2, there is no amplification of the perturbations (Q=1) for values of growth rate smaller than σ<-0.2. At these operating conditions (σ=-0.2), the surge margin values are below 5%. These low values of surge margin at which Q starts to grow are not suitable for application of this concept to industrial compressor design.

Furthermore the evaluation of DEB is computationally expensive because it requires the integration of the perturbations in the flow field along the compressor. For the incompressible dynamic model used in this thesis, the first harmonic of the least stable family of eigenvalues is in general the first eigenvalue to become unstable. Thus, considering only the growth rate of this eigenvalue is sufficient to assess the dynamic stability at a given operating condition. The new stability metric takes advantage of this statement to simplify the calculations. In addition, the previously developed dynamic stability metrics do not directly account for general changes in the shape of the compressor characteristic which is related to the robustness of the dynamic stability of the compression system to changes in operating conditions. This research also addresses this shortcoming and proposes a new stability metric based on dynamic considerations.

2.3 Motivation for a New Set of Stability Metrics Based on Dynamic Considerations

Chapter 1 briefly discussed the importance of meeting the required levels of dynamic stability throughout the operating envelope to avoid rotating stall and surge. To set the stage for a new stability metric, a more detailed treatment of the matter supported by numerical examples is presented in this section.

Currently, stable operation in the presence of inlet distortion, throttle changes and engine deterioration is achieved using surge margin. Surge margin is commonly defined in industry as:

$$SM_{Industry} = \left. \frac{\pi_{Surge} - \pi_{Operating}}{\pi_{Operating}} \right|_{Corrected\ mass\ flow} \tag{2.8}$$

Cumpsty [5] suggests that a more adequate definition of surge margin should consider the changes in outlet corrected mass flow between the operating line and the surge line. The advantage of this definition is that it provides a measure of the throttling

process necessary to take the compressor into stall. Surge margin as commonly defined by NASA captures this effect and is defined as:

$$SM_{NASA} = 1 - \left(\frac{\pi_{Operating} \times \dot{m}_{Corr,Surge}}{\pi_{Surge} \times \dot{m}_{Corr,Operating}} \right)\Bigg|_{Corrected\ Speed} \tag{2.9}$$

Since both definitions of surge margin are used in practice to determine compressor operability it is useful to compare the two for the same compressor. The compressor used to compare the two definitions of surge margin is a three stage generic compressor and the compressor map is shown in Figure 2-4. The operating line (solid) is chosen such that the surge margin is 20% per industry definition at all operating speeds.

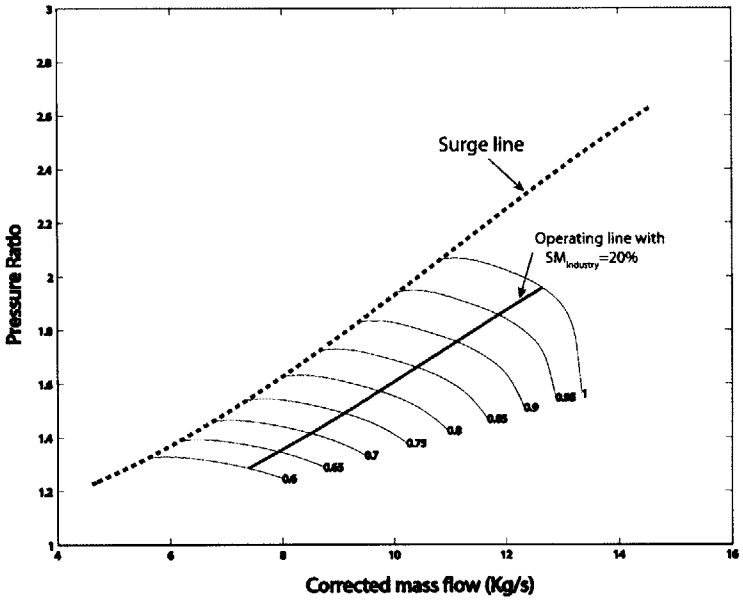

Figure 2-4. Compressor map for the 3 stage generic compressor with operating line with constant $SM_{Industry}$=20%

For the operating points illustrated in Figure 2-4, the surge margin per NASA and industry definitions are calculated to assess if the two definitions represent the same operability trends. In Figure 2-5 the values of the two definitions of surge margin are plotted at the operating points represented in Figure 2-4. While surge margin as defined by industry (solid) remains constant at all operating speeds, surge margin as defined by NASA (dashed) diminishes from a high level of 26% at 60% speed to a low level of 18% at 100% speed.

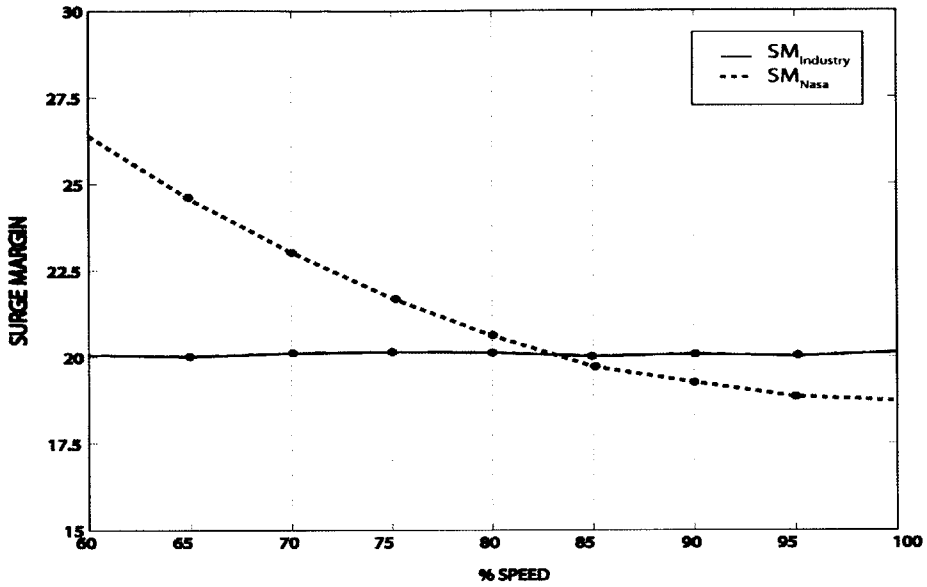

Figure 2-5. Surge margin as defined by industry (solid) and NASA (dashed) at different operating speeds for the generic 3 stage compressor with compressor map illustrated in Figure 2-4.

Since the two definitions of surge margin don't represent the same operability trends the question then arises which one of the two best represents the dynamic stability of the compressor and whether there is an alternate way to adequately capture compressor stability.

As discussed previously, the phenomena that govern the inception of surge and rotating stall are inherently dynamic and unsteady. It is thus suggested to investigate the growth rates of the small perturbations in the flow field that lead to instability at the different operating points illustrated in Figure 2-4. These results are then compared to the values of surge margin to assess if any of the surge margin definitions capture dynamic stability.

The Moore-Greitzer theory establishes that the growth rates of the perturbations in the flow field vary with the slope of the non-dimensional total-to-static pressure rise characteristic. As illustrated in Figure 2-4, the operating points present different slopes of the characteristics at different speeds. Thus, even if surge margin per the industry definition is constant throughout the operating envelope, one would expect the dynamic stability of the compressor to vary with operating speed. Figure 2-6 presents the values of the two surge margin definitions and the growth rate of the perturbations in the flow field calculated using Spakovszky's dynamic compressor model for the operating points indicated in Figure 2-4.

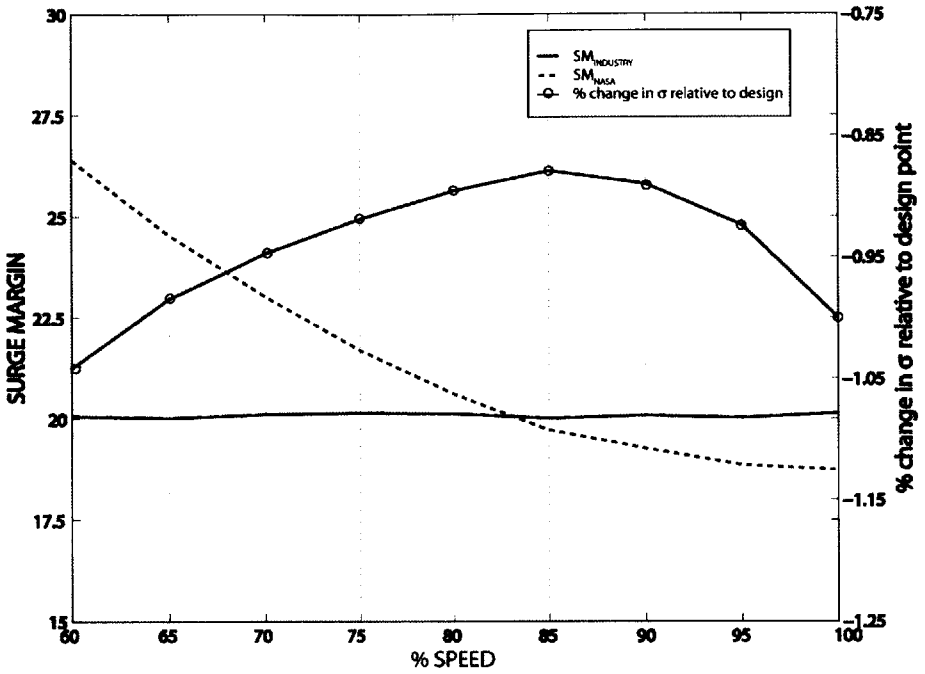

Figure 2-6. Surge margin as defined by industry (solid), and by NASA (dashed), and growth rate of the perturbations in the flow field (circles) at different speeds.

Figure 2-6 illustrates that both definitions of surge margin show a different stability trend compared to the growth rate of the perturbations (circles). This indicates that none of the two surge margin metrics correlate with dynamic stability and suggests an opportunity for a new metric. This result was expected since surge margin is a stability metric based on steady-state considerations with no direct physical link to dynamic stability. The evolution of the compression system resonances is further discussed next and a new stability metric is developed.

Additionally, Figure 2-6 suggests that at high and low speeds the compression system is overdamped and thus there is a potential for performance improvement. To illustrate this potential for performance improvement using dynamic stability a new operating line for the compressor illustrated in Figure 2-4 is calculated with the minimum allowable level of system damping throughout the operating envelope. The amount of system damping is chosen to be the minimum growth rate encountered along the operating line with constant SM=20% (i.e. σ=-0.65 at 85% speed). Figure 2-7 plots the compressor map for the 3 stage compressor with the two operating lines (constant SM=20% (solid) and constant σ=-0.65 (dashed)).

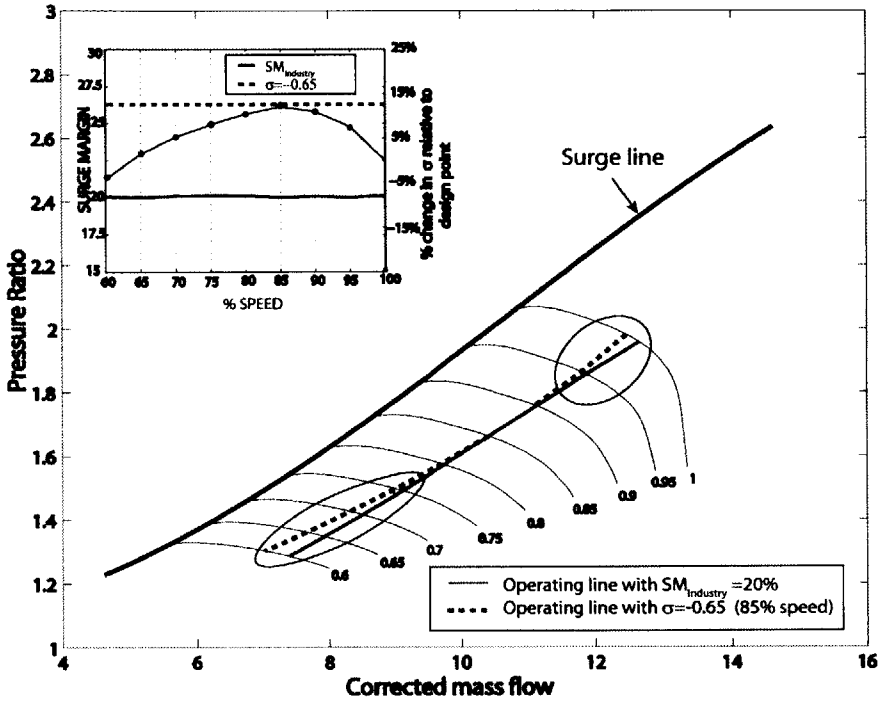

Figure 2-7. Potential for performance improvement if dynamic stability is considered.

A performance improvement at high and low speeds is suggested by lowering the excess level of the damping in the original operating envelope.

In both cases this example assumed the same compressor geometry with the purpose to illustrate the potential performance improvement using a dynamic based compressor stability metric. The question then arises how one would redesign the compression system for enhanced performance if the new stability metric was one of the primary design parameters. This is one of the main objectives of this thesis. To address this, a new stability metric based on compressor dynamic behavior is established.

2.4 Development of the New Stability Metric

The goal of this section is to define a new stability metric that represents the dynamic stability of the compression system. To illustrate the dynamic stability of a pumping system the mass-spring-damper mechanical analogue presented in Figure 2-8 can be considered (Greizer [13]).

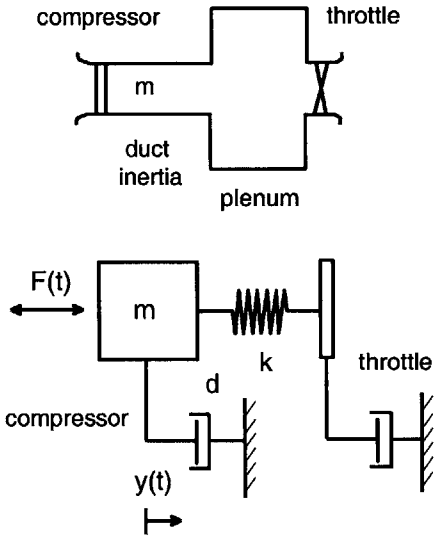

Figure 2-8. Mechanical analogue of a gas turbine system (adopted from [13]).

The damping of the compression system can be positive (removing mechanical energy from the system) or negative (adding mechanical energy to the system). The values of the compression system damping determine the amplifications of the natural resonances of the overall pumping system. The amplifications of the natural resonances are quantified by σ which, as was previously discussed, is directly linked to the slope of the pressure rise characteristic and thus depends on the blade rows performance characteristics. The idea is to calculate σ at the operating conditions of interest and to modify the blade row performance characteristics to obtain the desired values of compression system damping.

This section introduces the new stability metric based on dynamic considerations. The new metric should capture the dynamic stability of the compression system at operating conditions and also the robustness of the compression system stability to changes in operating conditions. After the metric is defined, a numerical example is given to illustrate the advantages of the new metric compared to surge margin.

2.4.1 Growth rate of the flow field perturbations

The first attribute of the new stability metric is that it should capture the dynamic stability of the compression system at a given operating condition. This can be

achieved by evaluating the temporal evolution of the growth rates of the perturbations in the compressor flow field at the desired operating condition. For example, the velocity perturbations are of the form

$$\delta v(t) \propto e^{(\sigma_n - jw_n)t} \tag{2.10}$$

The output of the dynamic compressor model is a set of eigenvalues of the form $s_n=\sigma_n-j\omega_n$, where σ_n and ω_n are the growth rate and the rotation rate of the n-th harmonic flow field perturbation or mode. As expressed in Equation (2.10), if σ_n is positive, the mode increases with time leading to surge and rotating stall. If on the other hand σ_n is negative, the perturbations in the compressor flow field decrease with time indicating that the compression system is dynamically stable. As illustrated in Figure 2-9, for the incompressible dynamic model used in this thesis, the first harmonic of the least stable family of eigenvalues is generally the first eigenvalue to become unstable[1]. Thus, considering only the growth rate of this eigenvalue is enough to assess the dynamic stability at a given operating condition.

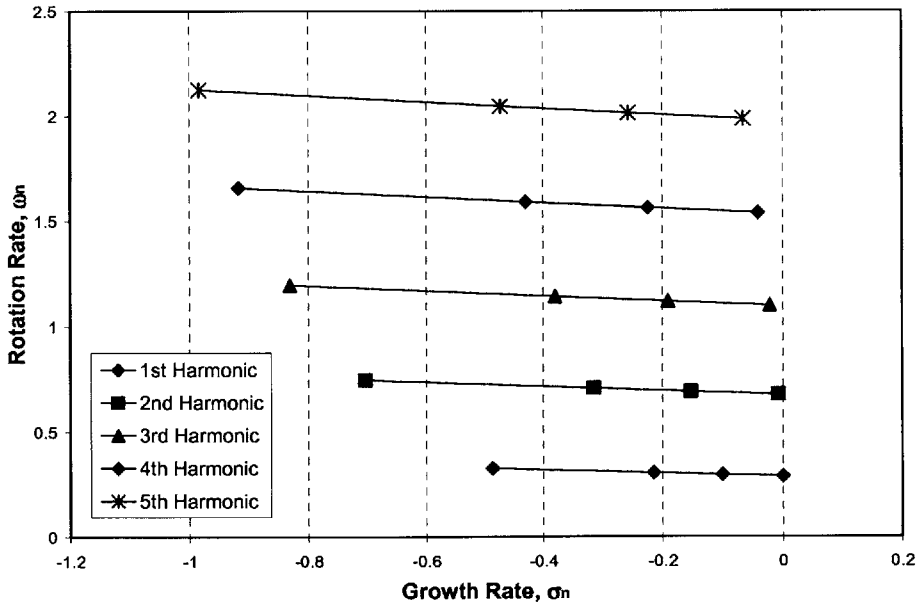

Figure 2-9. Eigenvalue map for the 3 stage compressor illustrating that the 1st harmonic of the least stable family of eigenvalues is the first mode becoming unstable.

[1] : An eigenvalue search algorithm is implemented to search for the least stable mode which determines overall compressor stability.

2.4.2 Robustness of the compression system stability to changes in operating conditions

The first attribute of the new stability metric ensures that an acceptable compression system damping is achieved throughout the operating envelope by changing the blade row performance characteristics so that slope of the pressure rise characteristic has an adequate negative value. The second attribute of the new metric is that it must guarantee adequate robustness of the compression system stability to changes in operating conditions. In order to illustrate the importance of this attribute the following example is considered.

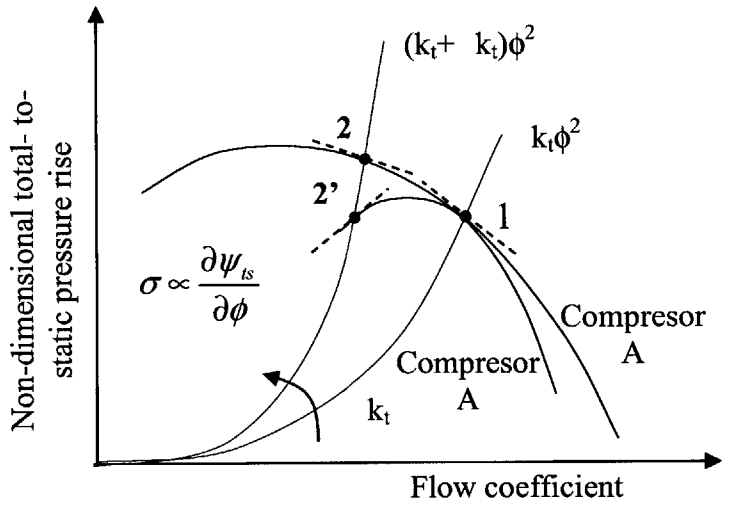

Figure 2-10. Robustness of compressor stability to changes in operating conditions.

In Figure 2-10, two compressor characteristics A and B are depicted and their stability behavior to changes in throttling coefficient is compared. According to the Moore-Greitzer model the growth rates of the perturbations in the flow field depend on the slope of the non-dimensional total-to-static pressure rise characteristic. As illustrated in Figure 2-10, the two compressors are initially operating with the same growth rate of the perturbations at point 1 (same slope). If the throttle coefficient is increased, as it might occur during an acceleration transient, the operating point shifts to operating point 2 for compressor A and operating point 2' for compressor B. The increase in throttle coefficient deteriorates the dynamic stability of compressor A which now operates at a condition with a less negative slope of the pressure rise characteristic.

However, after the change in operating conditions compressor B which has a steeper characteristic operates on the positively sloped side of the pressure rise characteristic such that the growth rates of the perturbations in the flow field at operating point 2' grow with time and thus compressor B becomes unstable. As illustrated in the example, the robustness of the compression system to changes in throttle coefficient depends on the shape of the compressor characteristic. A compressor characteristic with a higher curvature (compressor B) is more sensitive to operating changes than a compressor with low curvature (compressor A).

Thus, it is important to assess the shape of the pressure rise characteristic. This is achieved by calculating the local robustness of the compression system to changes in operating conditions at several operating points along the compressor characteristic. The metric to capture the robustness of the compressor can thus be defined as:

$$R = \left(\prod_{i}^{M} \left. \frac{\partial \sigma}{\partial k_t} \right|_{k_{ti}} \right)^{\frac{1}{M}} \tag{2.11}$$

where M is the number of discrete points along the compressor characteristic.

A large value of R indicates that the dynamic stability of the compression system deteriorates more rapidly with changes in operating conditions and thus is less desired.

2.4.3 New stability metric

The new stability metric is suggested to be a compound of the two attributes discussed and is defined as:

$$S_D = w_\sigma \left(\frac{\sigma}{\sigma_{\text{ref}}} \right) + w_R \left(\frac{R_{\text{ref}}}{R} \right), \tag{2.12}$$

and can be calculated according to:

$$S_D = w_\sigma \left(\frac{\sigma(k_{tdesign})}{\sigma_{\text{ref}}} \right) + w_R R_{\text{ref}} \left(\prod_{i=1}^{M} \frac{\sigma(k_{t_{i+1}}) - \sigma(k_{t_i})}{k_{t_{i+1}} - k_{t_i}} \right)^{\frac{1}{M}}. \tag{2.13}$$

The two attributes are normalized by adequate reference values and a weight assigned to each of the two effects so that one receives more importance over the other depending on the design philosophy adopted. In this thesis, the design philosophy is to

assign a larger weight to the growth rate of the perturbations across the operating envelope. Consequently, w_σ is given a value of 2/3 and w_R a value of 1/3 throughout the compressor map. Other design philosophies might yield different weights at different operating speeds. For example, a larger weight can be assigned to robustness at low speeds to account for the changes in operating conditions caused by engine accelerations. Furthermore, at higher speeds a larger weight can be assigned to the growth rates of the perturbations since at these operating speeds large engine accelerations are less frequent.

2.4.4 Example Application of the New Stability Metric

The benefits of the new stability metric compared to surge margin are demonstrated in this section using the following example. Consider two generic compressor maps, one with steeper speed lines (compressor A) across the compressor map and the other with shallow speed lines (compressor B) as illustrated in Figure 2-11. The surge line and the operating line are chosen such that both are the same for the two compressors. In addition, the surge margin as defined by industry is kept at 25% throughout the operating envelope. The objective is to illustrate that the new metric S_D captures the differences in the shapes of the compressor characteristics thus assessing the dynamic stability of the compression system while surge margin does not capture these differences in shape. Spakovszky's dynamic compressor model is used to evaluate the dynamic stability of the compression system at the operating points illustrated in Figure 2-11. To calculate the robustness R, two points (M=2) are used which correspond to operating points with 3% lower and 3% higher corrected mass flow relative to the working line. Then, S_D is evaluated using Equation (2.13) and the two definitions of surge margin are calculated using Equations (2.8) and (2.9)

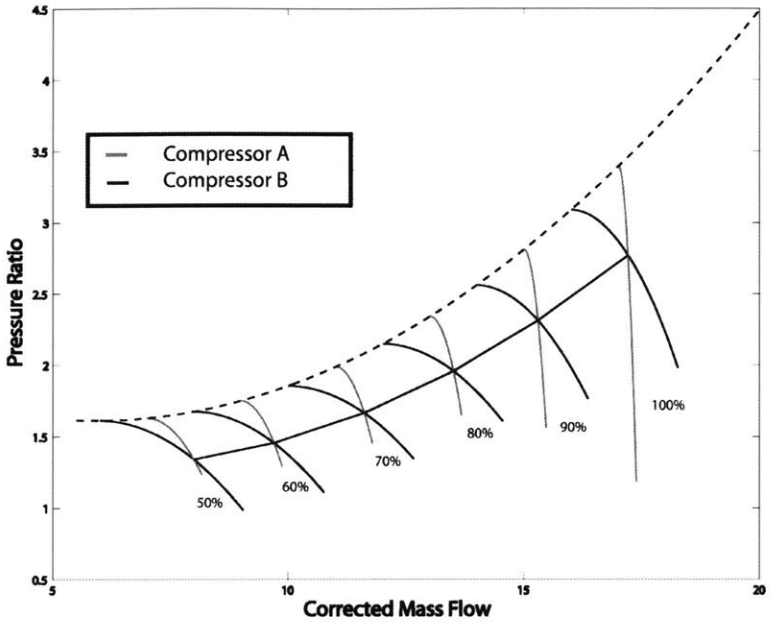

Figure 2-11. Compressor map illustrating two generic compressors with vastly different characteristics.

Figure 2-12 presents the surge margin results and evaluates the new stability metric S_D along the working line defined in Figure 2-11.

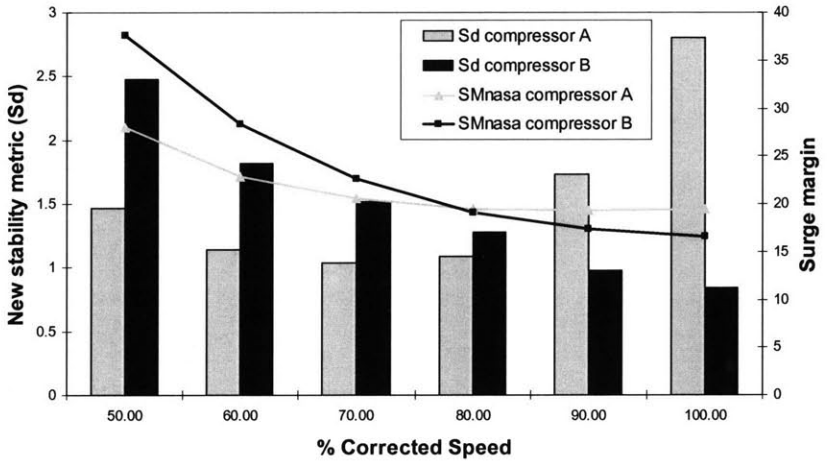

Figure 2-12. S_D versus SM_{NASA} for the two compressors considered in Figure 2-10.

For both compressors, surge margin as defined by NASA captures a decrease in stability as speed is increased. This decrease in surge margin is larger for compressor A than for compressor B. Additionally, the surge margin is the same for both compressors at 80% design speed. This indicates that at higher speeds surge margin as defined by NASA captures a higher level of stability for compressor A. The opposite is true at lower speeds.

S_D also captures a higher level of stability for compressor A over compressor B for operating speeds greater than 80% of design speed. However, the stability trends captured by surge margin as defined by NASA and S_D are not the same. In particular, for compressor A S_D captures a 3-fold increase in stability in the 80% to 100% speed range while surge margin per NASA definition remains constant over the same speed range.

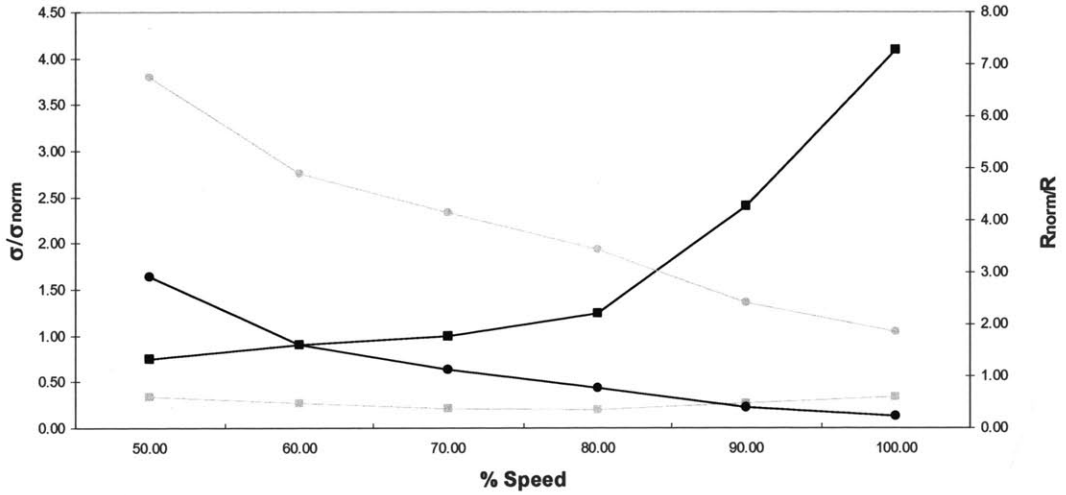

Figure 2-13. Growth rates and robustness for the two compressors considered in Figure 2-11.

To dissect the results, the two components of S_D are analyzed in Figure 2-13. Figure 2-13 illustrates that the contribution to S_D of the growth rates of the perturbations increases rapidly in the 80% to 100% speed range for compressor B. The new stability metric S_D is able to capture the improvement in dynamic stability of the compression system whereas surge margin as defined by NASA is not able to do so. Figure 2-13 also illustrates the differences in the two design philosophies behind compressors A and B. Compressor B is designed with moderate levels of growth rates of the perturbations and robustness across the entire compressor map. On the other hand, compressor B presents a low robustness R at low speeds to accommodate for engine accelerations. At higher speeds, where large changes in operating conditions are not expected, a large negative value of the growth rate of the perturbations ensures an adequate level of compressor stability. Ideally, as illustrated in figure 2-12, one would like a compressor to behave like compressor B in the 40% to 80% speed range and like compressor A at higher speeds. The choice of the compressor design philosophy depends on stability

considerations at low speeds and at high speeds and the compromises to be made between design and off-design conditions.

This example shows that surge margin as defined by industry does not correlate in any way with dynamic stability and that surge margin as defined by NASA follows qualitatively the stability trends shown by S_D. However, S_D captures the dynamic stability of the compression system and the sensitivity of stability to working line changes (i.e. shape of the characteristics) which neither of the two surge margins account for. Taking advantage of these features, the new stability metric, if used in the design phase as a prime design variable, suggests compressor designs with enhanced performance and dynamic stability. This is the focus of the remainder of the thesis.

2.5 Summary

This chapter demonstrates that neither of the two surge margin definitions used in the field to evaluate compressor stability correlate with dynamic stability. In addition, the potential for performance improvement is illustrated by removing the excessive damping levels in the compression system due to the current surge margin constraints. To take advantage of the shortcomings of the conventional stability metrics a new stability metric based on dynamic considerations (S_D) is defined. S_D is a compound of two attributes: the growth rates of the perturbations in the flow field (i.e. slope of the pressure rise characteristic) and the sensitivity of compressor stability to working line changes (i.e. shape of the pressure rise characteristic).

The advantages of S_D compared to surge margin are demonstrated using an example with two vastly different compressor characteristics. The results show that while surge margin per industry definition does not correlate with dynamic stability, surge margin per NASA definition can assess qualitatively some of the trends. However only the new stability metric S_D is able to quantitatively capture the dynamic stability of the compression system. This suggests to use S_D as the new metric throughout the remainder of this thesis in conjunction with a compressor design methodology to enhance compressor performance and stability.

Chapter 3

Fast Blade Performance Prediction Method

This chapter briefly motivates for the new fast blade performance prediction method and describes previous efforts using similar methodologies. Then, the three stepping-stones required to create the blade performance prediction method are discussed. These are the definition and the assessment of a new blade parameterization scheme. The generation of a blade performance database to define a new blade family, and the implementation of an N-dimensional linear interpolation to estimate the performance of a given blade row geometry. In addition, the accuracy and speed of the blade performance prediction method are compared to direct CFD simulations to assess the new approach.

3.1 Motivation

As discussed in Chapter 1, the preliminary compressor design phase entails the evaluation of the performance and operability of various compressor architectures. As discussed in Chapter 2, to calculate the dynamic stability of a compression system the slope of the blade row loss characteristics with respect to axial and tangential velocities is required (Equations (2.3), (2.4) and (2.5)). Consequently, to evaluate the compressor performance and stability the compressor blade row losses need to be calculated. These losses can be divided into profile losses and 3D loss effects such as for example end wall loss. One of the goals of this thesis is to develop a new compressor design methodology and to conduct proof-of-concept studies. To do so a 2D approach has been adopted. This assumption is appropriate since compressor geometries with high hub-to-tip radius ratios are considered where 3D loss effects are less important. These blade

row profile losses can be obtained either using experimental data or computational fluid dynamics (CFD). Since CFD allows a flexible design of cascade configurations and a fast evaluation of their performance, numerical simulations are used in this thesis to evaluate the profile losses of the different compressor configurations. Particularly, the blade-to-blade flow solver MISES [29] is used to do so.

The compressor optimization design based on the framework introduced in this thesis (Figure 1-8) requires the evaluation of the performance and stability of over one thousand compressor designs. If the profile losses of the compressor blade rows are evaluated using CFD in each iteration, the compressor optimization would require approximately 17 days. To reduce such a long turn around time a faster blade performance prediction method needs to be developed.

3.2 Previous Work

CFD based design methods use interpolation methods on previously gathered CFD information to estimate the performance of a given blade row. Perrot [21] proposes a CFD based method to predict the losses of an airfoil for different values of stagger. The method uses a least square fit of a surface to a set of CFD data points. The parameters considered are stagger angle and incidence angle and a surface fit according to:

$$\omega(i,\gamma) = c_0 + c_1 i + c_2 \gamma + c_3 i\gamma + c_4 i^2 + c_5 i^3 \gamma + c_6 i^4 \tag{3.1}$$

is used which allows twists and narrowings of the surface as the incidence and stagger angle are varied.

The results show that the discrepancy between the surface fit and the CFD data is too large for this methodology to be used in a compressor design optimization framework. Moreover, the method is limited to low Mach numbers (of order 0.1) and to variations in one geometric parameter (stagger angle varying in a ±3° range of the baseline value). Adding more geometric parameters and increasing the Mach numbers to open the design space and improve the performance of the optimizer requires a multi-dimensional surface fit which will further deteriorate the discrepancies between the CFD data and the surface fit.

Perrot's effort indicates that creating an accurate and fast method linking geometry, incidence and Mach number to blade performance is quite a challenge. The new CFD based method proposed in this thesis needs to be more accurate and needs to include more parameters than Perrot's method to enable performance and operability enhancement in the compressor design.

The approach is as follows. A blade parameterization is created and bounds on the geometric parameters are set to generate a new family of blades. Then the new family of blades is simulated using the blade-to-blade flow solver MISES and the blade performance information is stored using MATLAB to create a blade performance database. Finally, an N-dimensional linear interpolation between the blade performance files obtained from CFD is implemented which ensure accurate and fast blade performance estimates.

3.3 Blade Parameterization

The fast blade performance prediction method requires a family of blades to be generated. This blade family needs to represent various blade row designs such that the compressor design optimization framework can evaluate different compressor architectures. In addition the set of blades needs to include the minimum possible number of blade row geometries possible to reduce the CFD computational efforts. Consequently, a simple and versatile blade parameterization is required.

Sieverding et al. [23] propose a flexible blade parameterization to optimize an airfoil profile for minimum loss and maximum width of the loss bucket. The blade geometry is determined using 20 parameters. Two major inconveniences arise if this parameterization is considered to generate the required set of cascade geometries. The first problem is that the acceptable bounds on each of the 20 parameters are unknown with no a priori experience available on these parameters. Furthermore, the major disadvantage of this blade parameterization is that at least two sets (a lower and an upper bound) of each of the parameters need to be calculated to create a blade performance database. This implies that 2^{20} blades need to be simulated. Thus a simpler blade parameterization is needed to avoid the costly simulation of such a large amount of blades.

In gas turbine design practice, much simpler blade parameterizations are used to generate blade profiles. The most common families are the NACA 65 series, the British C series and double circular arc designs (DCA). Based on these, a simple parameterization was created to allow an effective blade profile definition using only a few parameters in order to generate a vast array of cascade geometries.

Next, the blade parameterization necessary to create the family of blades defining the blade performance database is discussed. Then, the blade parameterization is validated against previous design experience by assessing the impact on performance of changes around in an initial blade profile, stagger angle, camber angle, solidity and chord.

3.3.1 Blade Profile Definition

The following is a list of blade parameters commonly used to characterize compressor cascades:

- Chord (c).
- Stagger angle (γ).
- Camber angle ($\varphi=\chi_1-\chi_2$).
- Thickness to chord ratio (t/c).
- Thickness distribution (NACA, DCA, C4...).
- Blade solidity ($\sigma=c/s$).
- Blade pitch ($s=2\pi R/N_{Blades}$).

The above parameters are commonly used in compressor design practice and the new blade parameterization is based on these to generate the cascade geometry.

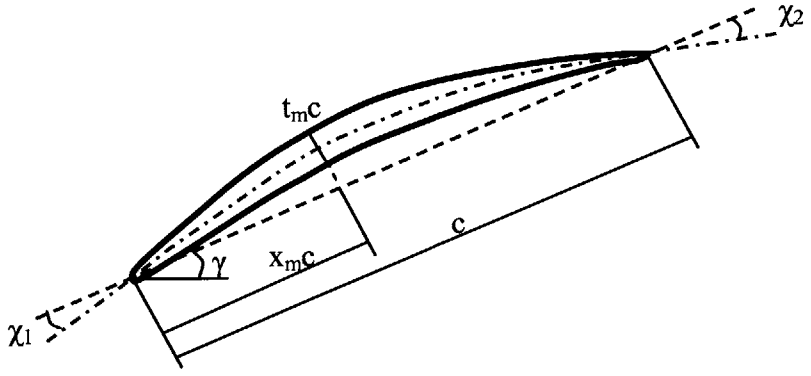

Figure 3-1.Parameters used to define the airfoil of a new family of blades.

The new family of airfoils is defined by 7 parameters:

- Chord, c.
- Maximum thickness to chord ratio, t_m=t/c.
- Percent chord location of maximum thickness, x_m.
- Unstaggered inlet metal angle or angle between camber and chord lines at inlet, χ_1. (χ_1 is always positive such that increasing χ_1 increases the camber angle).
- Unstaggered outlet metal angle or angle between camber and chord lines at outlet, χ_2. (χ_2 is always negative such that decreasing χ_2 increases the camber angle).
- Leading edge and trailing edge radii.

To define the cascade two additional parameters are introduced:

- Solidity, σ.
- Stagger angle, γ.

Figure 3-2 illustrates the generation of the cascade geometries. A thickness distribution is defined and added to a camber line to create the desired blade profile. Then, using solidity and stagger the blade profiles are arranged to define the cascade geometry.

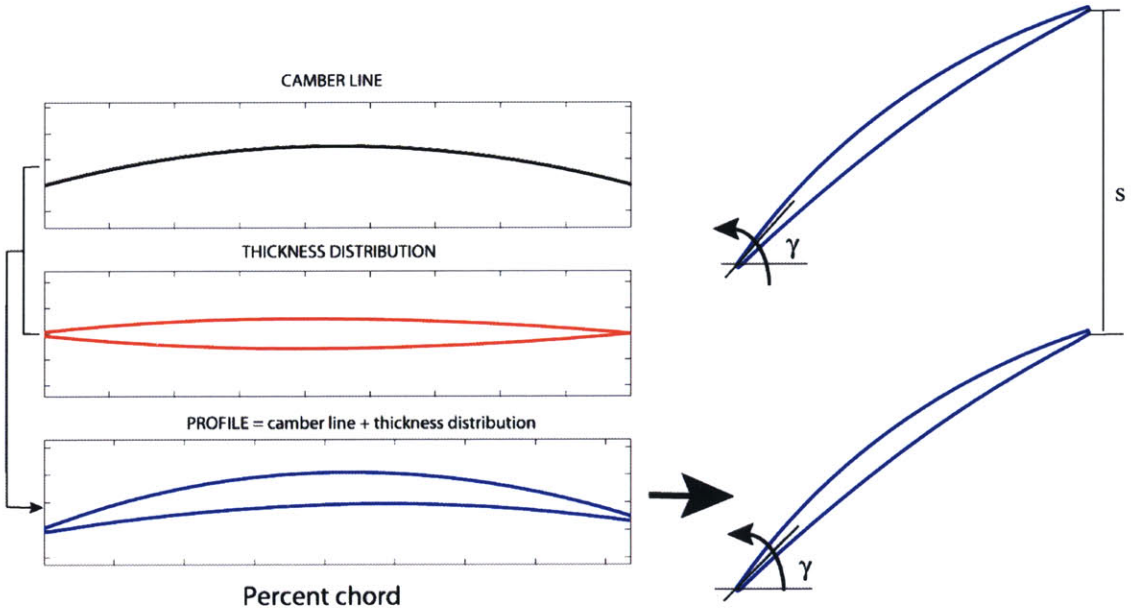

Figure 3-2. Generation of a blade profile (bottom left) by adding camber line (top left) to thickness distribution (middle left) and then staggering and applying blade pitch to define the final cascade (right).

The camber line is defined by a cubic polynomial using chord and inlet and outlet unstaggered metal angles:

$$\varphi_{line} = c_0 + c_1 x + c_2 x^2 + c_3 x^3 \ , \tag{3.2}$$

where c_0, c_1,c_2 and c_3 are the polynomial coefficients. In order to define the polynomial coefficients the following conditions are used:

$$\begin{aligned}
&\left.\frac{\partial \varphi_{line}}{\partial x}\right|_{x=0} = \tan(\chi_1) = c_1 \\
&\left.\frac{\partial \varphi_{line}}{\partial x}\right|_{x=c} = \tan(\chi_2) = c_1 + 2c_2 x + 3c_3 x^2 \\
&\varphi_{line}\big|_{x=0} = 0 = c_0 \\
&\varphi_{line}\big|_{x=c} = 0 = c_0 + c_1 c + c_2 c^2 + c_3 c^3
\end{aligned} \tag{3.3}$$

The advantage of this approach compared to other parameterizations is that it allows to directly vary the camber angle by modifying the inlet and exit unstaggered blade metal angles. For example, one can increase the camber angle near the leading edge by increasing χ_1, increasing χ_2 (i.e. decreasing its absolute value) which maintains the same level of blade profile camber.

The thickness distribution is defined by four parabolas which depend on chord, maximum blade thickness, position of the maximum thickness and the leading edge and trailing edge radii.

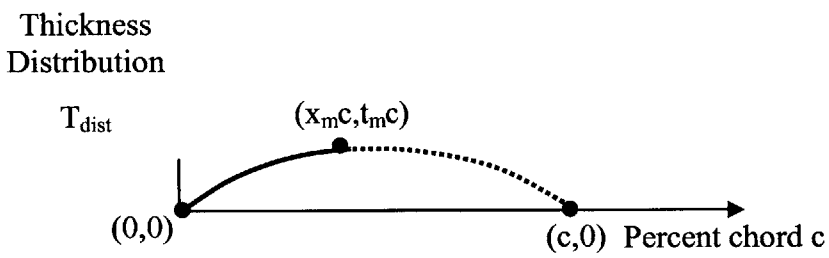

Figure 3-3. Thickness distribution defined with four parabolas. Two parabolas are used to define the top distribution (solid and dashed) and the other two for the bottom distribution (not shown).

The process used to define the four parabolas that form the thickness distribution is described below. The process is illustrated on one of the four parabolas.

$$T_{dist} = c_0 + c_1 x + c_2 x^2 \tag{3.4}$$

where c_0, c_1, and c_2 are the polynomial coefficients. In order to define the polynomial coefficients for the parabola illustrated in Figure 3-3 (solid line) the following conditions are used:

$$\begin{aligned} T_{dist}\big|_{x=0} &= 0 = c_0 \\ T_{dist}\big|_{x=x_m c} &= t_m c = c_0 + c_1 x_m c + c_2 (x_m c)^2 \\ \left.\frac{\partial T_{dist}}{\partial x}\right|_{x=x_m c} &= 0 = c_1 + 2c_2 x \end{aligned} \tag{3.5}$$

The advantage of this thickness distribution is that it defines the position of the maximum thickness which allows to explore blade profiles similar to the C series (defined with x_m=30%), the NACA 65 series (defined with x_m=40%) or the double circular arc family (defined with x_m=50%). This demonstrates the versatility of the blade parameterization used in this thesis.

Once the blade profile is generated, the blades are hinged at the leading edge and the appropriate stagger angle is applied. Finally the solidity is defined to assemble the blades into a cascade.

3.3.2 Effect of Geometric Changes on Blade Performance

Before the new family of blades is defined, the blade parameterization is assessed. The stagger angle, camber angle, solidity and chord of an initial cascade geometry are varied to assess the impact of these on blade performance. The initial cascade geometry is chosen with typical industry values so that σ=1.5, γ=30°, χ_1=15°, χ_1=-15°, c=0.045 m, t_m=5% and x_m=45%. Additionally, the impact on blade performance of variations in t_m and x_m is not investigated due to the limited impact on blade performance of these parameters in the range of interest.

3.3.2.1 Stagger Angle Effect on Blade Performance

This section discusses the impact of variations in stagger angle on blade performance. The stagger angle of the initial blade row geometry is varied by hinging the blade at the leading edge and varying the stagger angle from 20° to 36° in 2° steps. For each value of stagger angle the minimum level of loss is calculated and plotted in

Figure 3-4. Figure 3-4 illustrates that blade performance deteriorates with an increase in stagger angle.

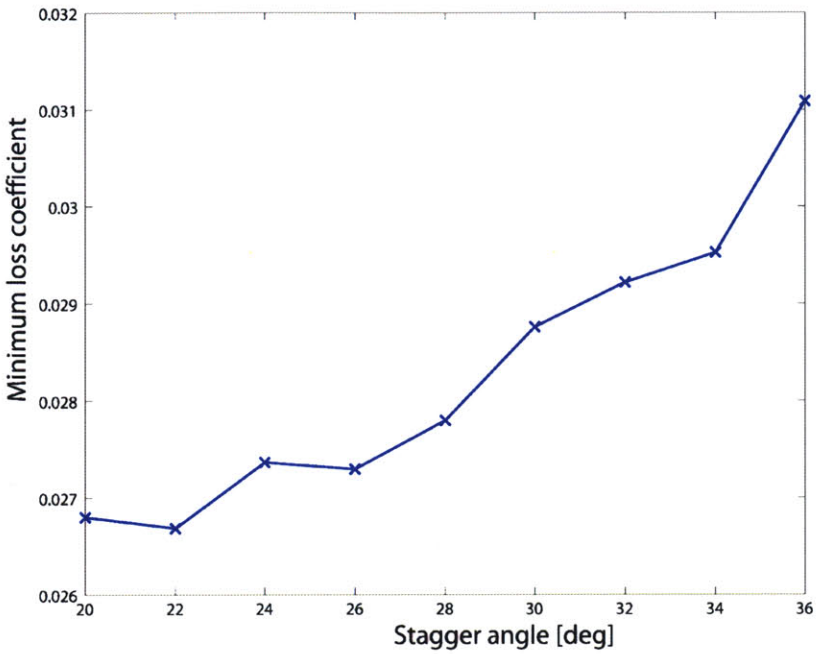

Figure 3-4. Minimum Loss versus stagger angle for a representative blade row geometry.

The deterioration of blade performance with increases in stagger angle is explained using Lieblein's diffusion factor [14]. Diffusion factor is commonly used to assess the performance of cascades because it correlates with momentum thickness and thus is representative of the state of the boundary layers inside the blade channel.

$$DF = 1 - \frac{V_2}{V_1} + \frac{\Delta V_\theta}{2\sigma V_1} \tag{3.4}$$

An increase in stagger angle in a cascade does not change the blade profiles but it does modify the diffusion area ratio. If stagger angle increases, the area ratio A_2/A_1 increases and thus the velocity ratio V_2/V_1 decreases (Perrot [21]). It can be seen from Equation (3.4) that an increase in stagger angle and thus an increase in V_2/V_1, leads to high diffusion factors. This indicates that the adverse pressure gradient in the blade passage and the blockage increase with increases in stagger angle leading to a deterioration in blade performance.

It is important to point out that a change in stagger angle does not modify the shape of the airfoils and consequently changes in incidence have a similar impact on cascades with different stagger angles. Figure 3-5 illustrates the loss buckets calculated at two levels of stagger angle (γ=20° and γ=36°).

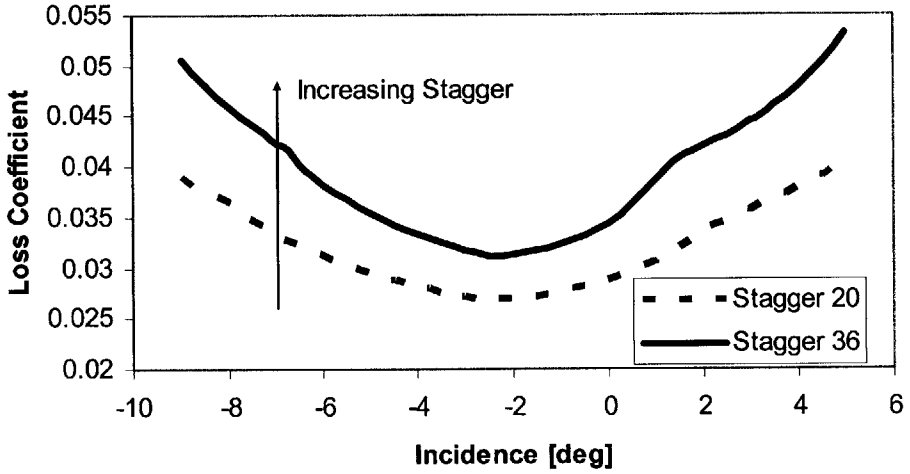

Figure 3-5. Loss buckets a representative blade row geometry for two levels of stagger angle (γ=20° and γ=36°).

Figure 3-5 illustrates that whereas an overall increase in loss results from an increase in stagger angle, the effect of changes in incidence are, as predicted, independent of stagger angle.

3.3.2.2 Camber Angle Effect on Blade Performance

An increase in camber angle increases the turning on the flow and thus raises the pressure rise of the cascade as expressed in Equation (3.5).

$$\psi = \phi(\tan(\alpha_1) - \tan(\alpha_2)) \tag{3.5}$$

Consequently, the adverse pressure gradient encountered by the flow increases as camber is increased. This causes the boundary layers to grow and if the adverse pressure gradient reaches a critical value the flow separates. Thus a deterioration of the cascade performance is expected with increases in camber angle. Equation (3.4) also captures the effect of camber angle on cascade performance. An increase in camber angle implies an increase in V_θ, which as expressed in Equation (3.4), raises the diffusion factor and deteriorates the cascade performance. To test if this trend holds in the new blade parameterization the camber angle of an initial profile is varied from

φ=24° to φ=36° and the minimum level of losses are calculated and plotted in Figure 3-6.

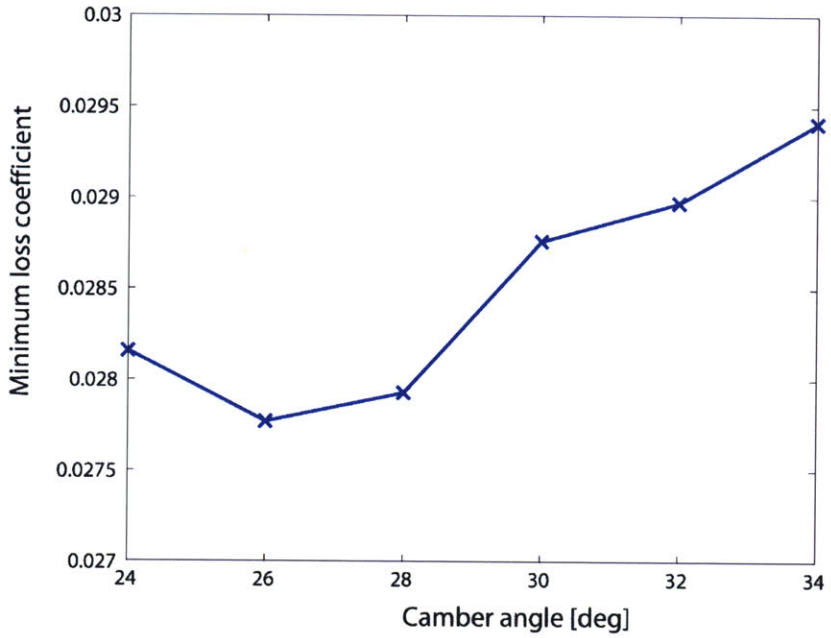

Figure 3-6. Minimum loss versus camber for a representative blade row geometry with camber angle varied between φ=24° and φ=34°.

The results depicted in Figure 3-6 show that increases in camber increase the minimum blade row loss and confirms the trends previously discussed. The impact of changes in incidence for the initial blade row geometry for two values of camber angle (φ=24° and φ=34°) is discussed next.

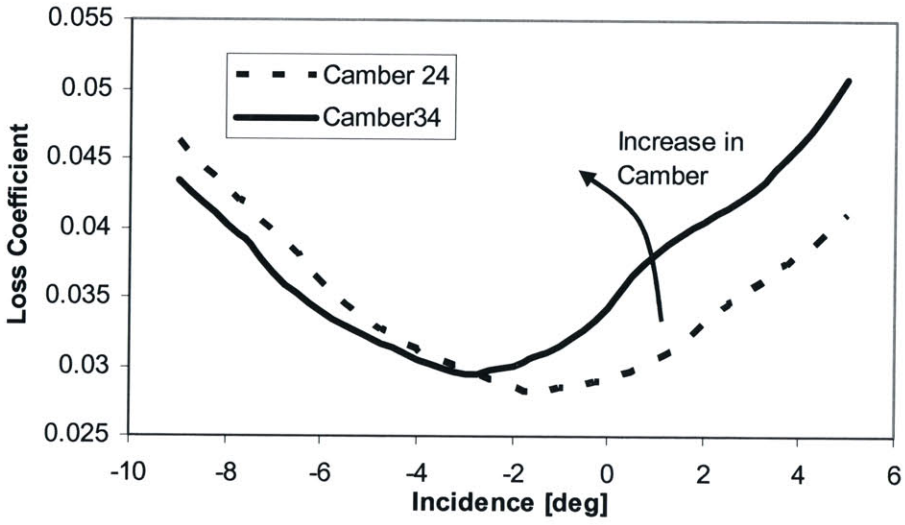

Figure 3-7. Loss buckets for a representative blade row for two different camber angles (φ=24° and φ=34°).

Figure 3-7 shows that if the camber angle of the initial blade row geometry is changed the blade row performance at negative incidence remains unaltered while the blade row performance at positive incidence deteriorates as camber increases. Operation at positive incidence yields a higher turning than at zero incidence and hence increases the pressure rise of the cascade. Thus for the situation where the camber angle is large and the adverse pressure gradient strong enough to provoke separation, an increase in incidence will have a more deleterious effect than compared to a blade with lower camber angle where the adverse pressure gradient remains relatively benign .

3.3.2.3 Effect of Solidity on Blade Performance

Solidity can be increased either by increasing the chord length or decreasing the blade pitch. Equation (3.4) establishes that the diffusion factor diminishes with increases in solidity. This improvement in cascade performance with increases in solidity can be explained by the decrease in the loading of the individual blades if their number is increased and the pressure rise of the cascade is kept constant. Additionally, the improvement in cascade performance can be explained by the reduction in adverse pressure gradient observed as chord is increased and pressure rise is kept constant. However, Equation (3.4) does not take into account the deterioration in blade row performance due to the increase in surface area in contact with the flow as solidity is increased.

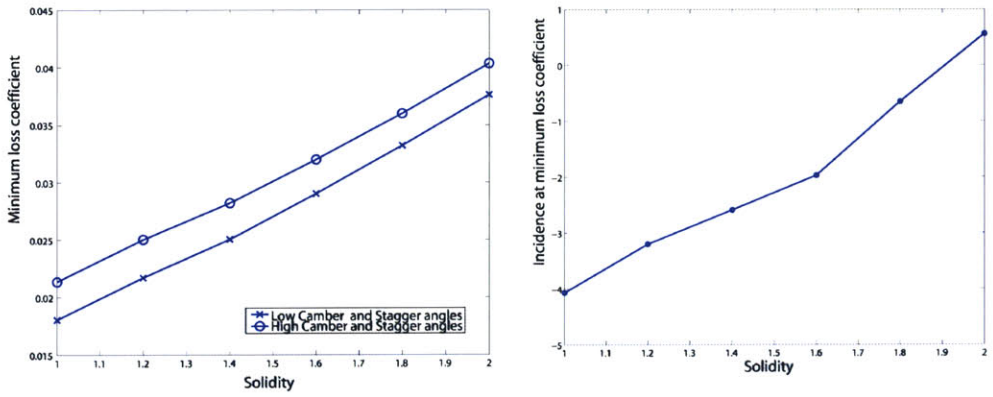

Figure 3-8. Effect of solidity on: minimum loss for a representative blade row geometry with different stagger angle and camber angle (left) and on incidence at minimum loss for the high stagger and camber angles case (right).

Figure 3-8 depicts two cascades where the solidity was modified by changing the number of blades. The results show that increasing solidity deteriorates blade

performance. Out of the three effects previously discussed, the increase in surface area in contact with the flow seems to be the dominant effect. Also, it was expected that the increase in solidity would have a larger beneficial effect on the cascade with higher stagger angle and camber angle. This is because the adverse pressure gradient in this situation is strong enough to cause separation and an increase in solidity decreases the loading of the individual blades. Figure 3-8, shows that the impact of changes in solidity on cascade performance is the same for both the high and the low stagger angle and camber angle cases. Consequently, the decrease in the loading of the individual stages with increases in solidity does not have a substantial impact on blade performance. Figure 3-8 (right) also shows that the incidence at minimum loss moves towards the positive incidence side as solidity is increased. This is beneficial because as solidity increases the operating condition where the cascade performs best is also the condition where more turning of the flow, and thus more work, can be obtained.

3.3.2.4 Effects of Chord on Blade Performance

Two opposing effects on cascade performance occur if the blade chord is changed. A decrease in chord length decreases the surface area in contact with the flow and improves the cascade performance. However, if the camber angle is kept constant, a shorter chord length implies that the flow has to turn over a shorter length to provide the same pressure rise. This increases the adverse pressure gradient in the cascade and deteriorates the blade row performance as chord is decreased.

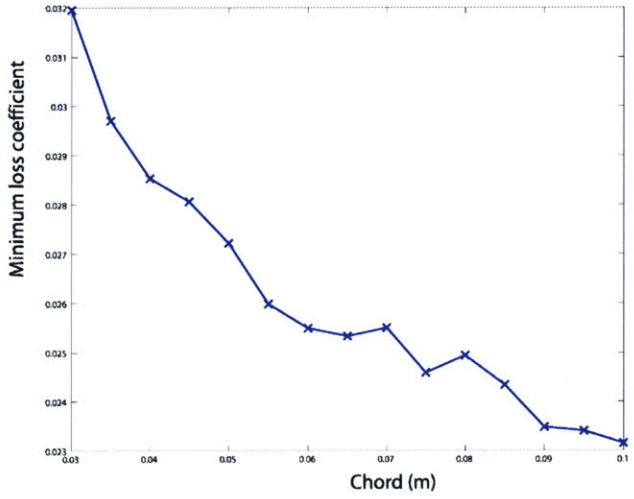

Figure 3-9. Effect on minimum losses of changes in chord for a representative blade row if chord is varied from c=0.03 m to c=0.1 m.

The blade chord of the initial geometry is varied from c=0.03 to c=0.1 and for each of the cases studied the minimum level of loss is calculated. Figure 3-9 shows that an increase in chord is beneficial. Consequently, in the example considered, this indicates that reducing the adverse pressure gradient has a larger impact on cascade performance than increasing the surface area in contact with the flow.

3.4 Blade Performance Prediction Method

The blade performance prediction method uses an N-dimensional linear interpolation between the blade performance files obtained from CFD to estimate the performance of a given geometry.

Having established the blade parameterization, the family of blades necessary to generate the blade performance database needs to be defined. This requires a choice of the range in geometric parameters that define the blade family. Then, the blade row geometries are simulated using an automated blade-to-blade CFD utility (MISES). Finally the N-dimensional linear interpolation method is implemented to predict the performance of the desired cascade geometry. Last, the accuracy of the new performance prediction method is assessed.

3.4.1 Blade Family

The ranges of the geometric parameters used to define the family of blades used in this thesis are summarized in Table 3-1. The range in geometric parameters is based on compressor design practice and on the limits of the convergence of the CFD method used in this thesis.

	χ_1 [deg]	χ_2 [deg]	Chord (m)	Solidity	Stagger angle [deg]	x_m (%)
Minimum Value	10	-15	0.03	1.5	20	30
Maximum Value	20	-10	0.05	2	35	50
Number of points between bounds	4	1	3	1	6	1

Table 3-1. Recommended ranges of geometric parameters to define the blade family.

In addition, Table 3-1 suggests the number of points between the bounds of each parameter to be simulated. These are the values used throughout this thesis and are chosen based on the experience gained with the blade performance prediction method in this research and the computer power available. More points between bounds imply a higher discretization of the ranges of parameters and thus a higher resolution of the linear interpolation method. However, a higher discretization of the ranges of parameters requires a larger computational effort. Consequently, the final discretization of the range in geometric parameters to be simulated will depend on the computer power available and the time allotted for the generation of the blade performance database.

3.4.2 Automated CFD utility

In order to generate the blade performance database for the newly defined family of blades, the blade-to-blade flow solver MISES [28] is used. This blade-to-blade flow solver solves the steady Euler equations coupled with a turbulence model and a boundary layer model using a full Newton method on an intrinsic streamline grid for the desired blade row geometry.

Furthermore, since the number of blade row geometries to be simulated might be large, Matlab is used to automate the process. The procedure used to simulate one blade profile is outlined in Figure 3-10.

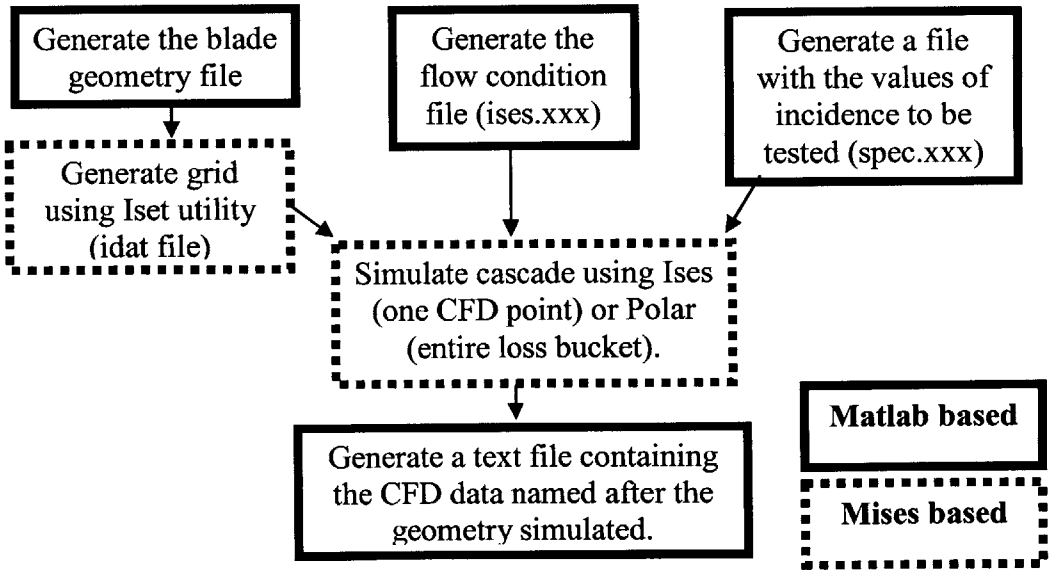

Figure 3-10. Diagram showing the different steps necessary to generate one cascade performance file.

Figure 3-10 illustrates the different steps required to obtain a blade performance file. Initially, the coordinates of the blade, the flow conditions (Mach number and Reynolds number) and the incidence angles are written into three files using Matlab. Then, the grid is generated using the blade geometry file. The result is a file (idat) containing the grid information. Then, Ises or Polar calculate the performance of the cascade using the grid file (idat), the flow condition file (ises) and the file containing the incidence angles to be simulated (spec). Once the performance of the cascade is calculated, the output file from MISES is opened using Matlab and the data is rewritten into a text file containing incidence, Mach number and performance information. This file is named after the geometry that was simulated. Then, the process is repeated for all cascade geometries to generate the blade performance database to be used by the interpolation method in the compressor design optimization framework.

3.4.3 Interpolation Method

In order to predict the performance of a given blade row geometry an N-dimensional linear interpolation between the blade performance files is implemented. The method is effective since it provides the necessary blade performance estimates in less than 0.1 seconds. This is 1/100 of the average time required by MISES to calculate one operating point. Furthermore, the blade performance prediction method must provide accurate results since the fidelity of the blade performance prediction method is crucial to the overall success of the optimization framework. This is discussed next.

3.4.4 Resolution of the blade performance prediction method

The results of the blade performance prediction method need to be as accurate as possible. This is important because during the optimization process many compressor designs are evaluated and a small inaccuracy in the performance calculation at the beginning of the compressor optimization can lead to an inadequate compressor design at the end of the process.

To assess the accuracy and fidelity of the blade performance prediction method, the blade row losses of the baseline 3 stage compressor which are used throughout this thesis (refer to Chapter 4 for more details on the compressor geometry) are directly calculated using MISES and are compared to the predictions using the blade

performance prediction method (N-dimensional linear interpolation based on blade row database generated using MISES). Figure 3-11 presents the blade row losses as a function of incidence at design speed as mass flow is varied from choke to stall. The results using the fast blade performance method are marked by the solid lines and the direct MISES simulation results are marked with dashed lines.

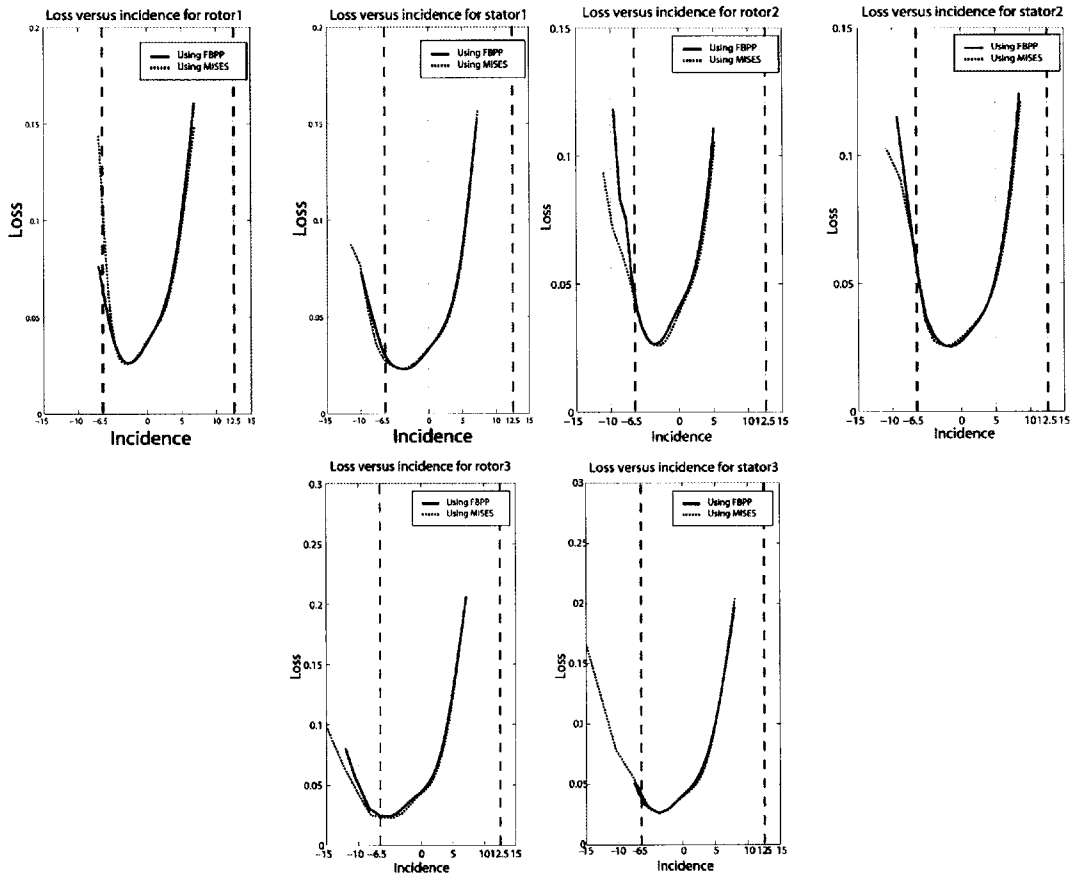

Figure 3-11. Prediction of loss versus incidence for a generic three stage compressor using direct CFD simulations (dashed) and the fast blade performance prediction method (solid).

Figure 3-11 shows that the values of the losses for the ranges of incidences to be considered are practically the same for both methods. Typically, the discrepancy between the direct CFD results and the blade performance prediction method is less than 1% and only small variations in the slopes of the loss buckets are observed. This discrepancy in slope does not affect the pressure ratio and efficiency calculations. However, the discrepancy in the calculated slopes has an impact on the calculation of the growth rate σ and robustness R which are necessary to calculate the new stability

metric S_D. Furthermore, the calculation of R requires the evaluation of the change in σ with respect to throttle coefficient.

To assess the impact of the small discrepancies between the direct CFD and the blade performance prediction method on the objectives of compressor design optimization , the performance and dynamic stability of the compressors considered in this thesis are assessed using both methods.

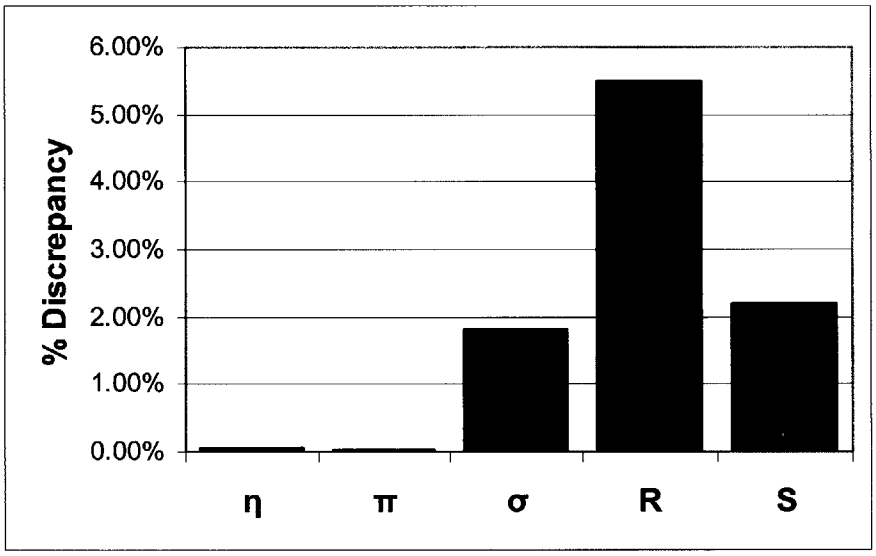

Figure 3-12. Averaged discrepancy in performance and stability between direct CFD simulations and performance prediction method for the 4 compressors simulated in this thesis.

Figure 3-12 presents the average discrepancy between the direct CFD simulations and the blade performance prediction method for the compressors used in this thesis. The results in pressure ratio and efficiency show no discrepancy due to the small differences in loss between both methods. As mentioned earlier, evaluating σ requires the calculation of the slope of the loss buckets. This increases the discrepancy in σ to 2%. Additionally, the calculation of the robustness R requires the derivative of σ with respect to throttle coefficient. This further increases the discrepancy between both methods to a value of 5.5%. However, this 5.5% discrepancy is never directly introduced in the optimization loop because R is only used in unison with σ to calculate S_D. Consequently, the maximum discrepancy introduced in the optimization loop is 2%, a value low enough to avoid misleading search directions in the optimization.

The results of the blade performance prediction method demonstrate that the method is accurate enough (maximum discrepancy with CFD <2%) and very effective

(100 times faster than MISES) and is used to estimate the blade row performances in the compressor design optimization framework.

Chapter 4

Compressor Design Optimization of a Generic 3 Stage Compressor

The objective of this chapter is to implement and to apply the compressor design optimization framework to a 3 stage baseline compressor. The goal is to demonstrate, as conjectured in Chapters 1 and 2, that a performance improvement can be obtained if dynamic stability is used as a prime design variable in the compressor design optimization framework. This chapter is organized in four sections. First, previous compressor optimization efforts are discussed and the advantages of the new approach are described. Then, the inputs, outputs, assumptions and limitations of the different modules used in the compressor design optimization framework are introduced. Next, the 3 stage test compressor is defined and the baseline compressor performance and stability are evaluated at different operating speeds. The new compressor design optimization framework is then applied to the 3 stage compressor using two different optimization strategies. The objective of the first optimization strategy is to improve the compressor efficiencies at high speeds where a low specific fuel consumption is desired. The second optimization strategy has the purpose to enhance the compressor dynamic stability to improve the matching of the compressor stages at design and off-design conditions.

4.1 Previous Work

The compressor design optimization framework developed and used in this thesis is based on Perrot's [21] framework. Perrot used surge margin as one of the prime design objectives and demonstrates a 6% improvement in surge margin at design conditions at the cost of a 0.5% drop in efficiency and a 2% decrease in pressure ratio

for a 3 stage compressor. The new optimization framework improves Perrot's work in several aspects. Instead of a single point optimization the new framework allows the design optimization across the entire compressor map, i.e. objectives functions can be specified at various speeds, to tailor and to improve the matching of the compressor stages at design and off-design operating conditions. Additionally, the new blade performance prediction method (see Chapter 3 for details) is capable to efficiently predict the blade performance as a function of multiple blade geometric parameters (7 used in this thesis) compared to only 1 parameter in Perrot's formulation. This introduces more freedom in the search for the optimal blade row and compressor configuration which potentially could enable enhanced compressor performance and operability. Furthermore, the new compressor design optimization framework is based on dynamic stability and uses the new metric S_D to assess stability. This offers to further improve compressor performance as illustrated in Chapters 1 and 2.

4.2 Novel Compressor Design Optimization Framework

The compressor design optimization framework consists of three modules: the optimization module, the fast blade performance prediction module and the compressor flow field simulation module. The optimizer assesses if the user defined objectives and constraints are satisfied. The objective of the optimization is to define the desired attributes of the compressor to be optimized and thus represent the design philosophy to be used. If the objectives and constraints are not met, the optimizer modifies the compressor geometry and tries to provide an improved compressor design. Then, the compressor flow field simulation code evaluates the performance and stability of the new compressor geometry throughout the operating envelope. In order to calculate the compressor performance and stability the performance of the individual blade rows needs to be predicted. Consequently, the fast blade performance prediction method is used together with the flow field simulation code to calculate the compressor performance and stability. Finally, if the optimization objectives and constraints are satisfied the optimal compressor design is obtained. Otherwise, the optimization loop is repeated until the final optimal design is reached.

The inputs, assumptions and limitations of the compressor design optimization framework modules are described next.

4.2.1 Compressor Flow Field Simulation Code

The flow field simulation code is divided into two parts: a mean-line flow calculation and a dynamic stability calculation. A similar mean-line flow solver was previously used by Dorca [7] and Perrot [21]. It calculates the compressor performance in terms of overall pressure ratio and adiabatic efficiency and the uniform time-mean flow field quantities that are required to compute the unsteady flow field perturbations and dynamic stability. The inputs to the mean-line flow solver are:

- Number of compressor stages
- Hub and tip radii for each blade row
- Compressor inlet conditions (temperature and pressure)
- Compressor inlet mass flow
- rotor speed
- Blade row and gas path geometry (γ, χ_1, χ_2, σ, c, t_m and x_m for each of blade rows).

The mean-line flow calculation neglects 3D loss effects. This limits the application of the mean-line flow solver to compressor stages with high hub-to-tip radius ratios. In addition, the deviation effects are accounted for using empirical correlations valid for operating conditions near zero incidence operation.

Using the steady background flow field from the mean-line calculation and blade row loss characteristics the dynamic compressor stability model computes the compressor pre-stall modes, or natural frequencies of the flow field perturbations. The growth rate σ of the least stable mode is determined to calculate R and S_D as discussed in Chapter 2. More specifically, the inputs to the dynamic compressor stability model are:

- Number of compressor stages
- Axial chord length of each of the blade rows, inlet and outlet duct lengths and inter blade-row gap lengths

- Uniform background flow field quantities (non-dimensional axial and tangential mean velocities and inlet and outlet flow angles).
- Sensitivity of blade-row loss changes in the non-dimensional axial and tangential velocities ($\partial L/\partial V_{x1}$ and $\partial L/\partial V_{\theta 1}$).
- Unsteady loss term accounting for the time lags in the unsteady loss model

A more detailed description of the assumptions used in the dynamic compressor model is discussed in Chapter 2.

4.2.2 Fast Blade Performance Prediction Method

The fast blade performance prediction method consists of a blade performance database established using MISES and an N-dimensional linear interpolation method to effectively and accurately estimate the blade row losses. To generate the blade performance database a new blade family is defined as discussed in Chapter 3.

The inputs to the blade performance prediction calculation are:

- Blade row geometry (γ, χ_1, χ_2, σ, c, t_m and x_m).
- Relative Mach number into the blade row
- Incidence angle into the blade row

The following range of parameters is used to define the blade row family database to be used in the optimization of the 3 stage baseline compressor. The number of discrete points between each of the bounds was chosen based on the computer power available and the experience gained using the method with different combinations of points between bounds.

	χ_1[deg]	Stagger angle [deg]	Incidence angle [deg]	Inlet Mach number
Minimum Value	12	25	-6.5	0.1
Maximum Value	23	35	12.5	0.78
Number of points between bounds	10	4	36	32

Table 4-1. Range in incidence, Mach number, stagger angle and unstaggered inlet metal angle considered to generate the blade performance database.

Table 4-1 presents the range in incidence, Mach number, stagger angle and unstaggered inlet metal angle included in the blade performance database considered.

Other parameters such as gas path radii, chord length, and solidity can be included without major implementation but for simplicity only Mach number, incidence, stagger angle and unstaggered inlet metal angle were varied in the cases investigated.

4.2.3 Optimizer

This section describes the algorithm used by the optimizer and the optimization problem set-up (i.e. objective functions and constraints) required to start the optimization tool.

4.2.3.1 Algorithm

A gradient-based method is used to search the design space for an optimal compressor design. Specifically, the sequential quadratic programming algorithm (SQP) implemented in Matlab's optimization toolbox is used (fmincon function). At the start of each optimization loop, gradient-based search methods use the information in the gradient matrix to obtain a new search direction that maximizes the user defined objective function and satisfies the constraints of the optimization problem.

The SQP algorithm is widely used in engineering applications and is adequate for constrained and non-linear optimization problems. This is well-suited for the highly constrained compressor design optimization because the operating incidences need to be within the incidence bounds set by the blade performance prediction method and some minimum requirements in pressure ratio, efficiency and stability need be satisfied.

Also, the sequential quadratic programming algorithm is appropriate for the compressor design optimization because the relationship between geometry, performance and dynamic stability is non-linear (for more details on the principles of the SQP algorithm see Willcox [25]).

Three inputs are provided to the SQP algorithm: the objective function (i.e. pressure ratio, efficiency or stability), the independent variables (i.e. compressor geometry) and the optimization constraints (i.e. minimum requirements for the objective function and incidence bounds).

4.2.3.2 Objective Function Used in the Compressor Design Optimization

Depending on the compressor design philosophy, the compressor optimization objectives might be set up differently. For example, over the past four decades designing for maximum efficiency has been the driver of most compressor design optimizations (Greitzer and Wisler [11]). In the compressor optimizations for maximum efficiency one would want to optimize for maximum efficiency at high speeds where low specific fuel consumption is desired. Additionally, current compressor design efforts are also geared towards the reduction of compressor flow field instabilities throughout the operating envelope. Thus, one might also want to optimize for maximum stability at design and off-design operating conditions to ensure the adequate matching of the compressor stages and to avoid the use of variable geometries and bleed valves. Since the compressor design philosophy is case dependent, a versatile objective function representing the most relevant design philosophies (i.e. enhancing pressure ratio, efficiency and stability) is created. In particular, the compressor geometry can be optimized for maximum pressure ratio, stability or efficiency at one or several operating speeds. Weighting factors (ξ) can be assigned to each of the objectives at the different operating conditions. This favors improvements in the compressor design in the operating regions of interest. Furthermore, one can create an objective function including any weighted (p) combination of the previous objective functions. This objective function is in general of the form:

$$\mathrm{OBJ}= p_{\pi}\times\left(\sum_{Speed}\xi_{\pi Speed}\frac{\pi_{Speed}}{\pi_{iSpeed}}\right)+p_{\eta}\times\left(\sum_{Speed}\xi_{\eta Speed}\frac{\eta_{Speed}}{\eta_{iSpeed}}\right)+p_{S_D}\times\left(\sum_{Speed}\xi_{S_D Speed}\frac{S_{D\,Speed}}{S_{D\,iSpeed}}\right) \quad (4.1)$$

where all the objectives are normalized by their baseline values, ξ is the weighting factor assigned to the individual objectives at different speeds and p is the weighting factor used for the compounded sum of the pressure ratio, efficiency and dynamic stability objective functions.

4.2.3.3 Constraints of the Compressor Design Optimization

Constraints are used to ensure that the operating incidences are within the incidence bounds where the fast blade performance prediction method generates

accurate results. As discussed in Chapter 3, this is important because a small discrepancy in the compressor performance and stability calculations at the start of the compressor design optimization process might lead to sub-optimal compressor geometries. In addition, constraints are included to guarantee a certain minimum level of efficiency and stability across the operating envelope. Finally, bounds on the operating line in terms of the maximum and minimum working line pressure ratio are included to ensure that the demands of the turbine are satisfied.

4.2.3.4 Independent Variables of the Compressor Design Optimization

The variables of the compressor optimization problem are the absolute exit metal angle of the IGV upstream of rotor 1 and the geometric parameters required to generate the blade row geometries and the gas flow path. For simplicity, in this thesis only the exit metal angle of the fixed geometry IGV, the stagger angle and unstaggered inlet metal angles of the individual blade rows are introduced as independent variable. Thus, the optimization problems of the 3 stage baseline compressor considered in this thesis includes 13, independent variables ($2\times6+1$).

4.3 Baseline 3 Stage Compressor

The baseline compressor geometry used in this thesis is designed such that the compressor stability remains constant throughout the operating envelope. As discussed in Cumpsty [5], this can be achieved by setting the incidences at design speed to negative values in the front stages and to positive values in the rear stages since, as the operating speed is reduced from design speed, the flow coefficients along the compressor change. The result of a reduced operating speed is that the front stage operating conditions shift towards positive incidences (or stall) and the rear stages operating conditions shift towards negative incidences (or choking).

	R1 [deg]	S1 [deg]	R2 [deg]	S2 [deg]	R3 [deg]	S3 [deg]
100%	-5.28	-6.49	-2.84	0.88	3.28	6.48
90%	-2.96	-4.56	-1.46	1.45	3.17	5.76
80%	-0.53	-2.57	-0.17	2.04	3.19	5.26
70%	1.57	-0.89	0.94	2.60	3.24	4.84
60%	3.28	0.50	1.83	3.04	3.25	4.43
50%	4.79	1.71	2.67	3.46	3.35	4.15
40%	5.86	2.60	3.21	3.72	3.31	3.84

Table 4-2. Incidence angle [deg] into the different blade rows as a function of rotor speed for the baseline compressor.

Table 4-2 summarizes the operating incidences for the baseline compressor blade rows at different operating speeds and illustrates the shift in operating incidences of the blade rows as operating speed is changed.

The baseline compressor geometry used to generate this distribution of incidences is a 3-stage compressor with identical geometries for all its blade rows. The blade row geometries is chosen to be defined by $\gamma=30°$, $\alpha_1=17°$, $\alpha_2= -15°$, $\varphi=30°$, $c=0.045$ m ,$\sigma=1.5$, $t_m=5\%$ and $x_m=45\%$. The gas path is adjusted to achieve the desired flow coefficients (i.e. incidence angle) through the compressor and is plotted in Figure 4-1.

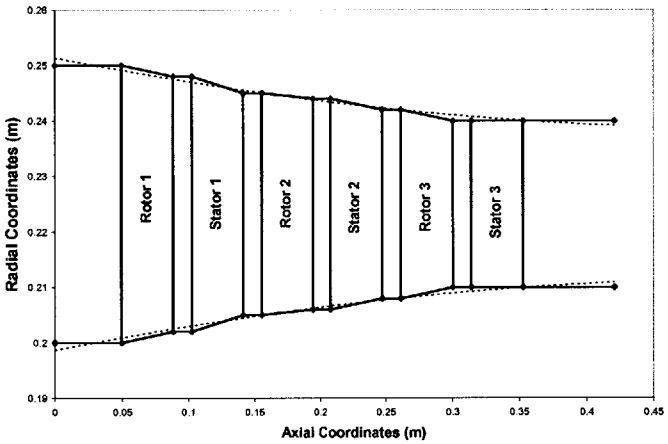

Figure 4-1. Gas flow path of the 3 stage baseline compressor.

The baseline compressor performance and stability are calculated across the compressor map using the compressor flow field simulation module. The results are summarized in Table 4-3 and the compressor map and efficiency curves are plotted in Figure 4-2. The operating speeds of interest are: the idle condition (40% speed), the end

of cruise condition (80%), the design condition (90% speed) and the maximum climb condition (100% speeds).

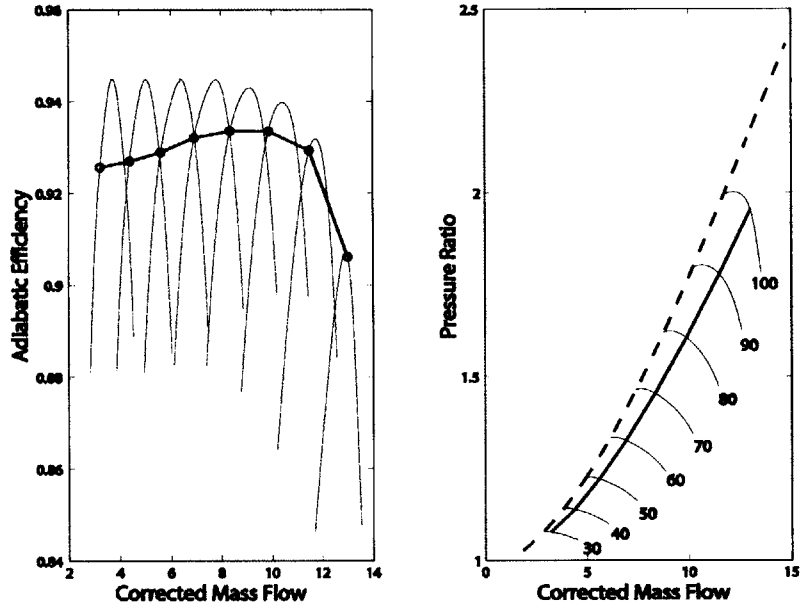

Figure 4-2. Compressor map and efficiency curves for the 3 stage baseline compressor.

SPEED	η (%)	π	σ	R	S_D	SM_{NASA} (%)
100	90.54	1.95	-0.75	1.47	1.08	11.12
90	92.89	1.78	-0.50	0.63	0.91	11.09
80	93.26	1.61	-0.49	0.39	1.06	11.08
70	93.23	1.46	-0.49	0.30	1.19	11.22
60	93.07	1.33	-0.48	0.26	1.27	11.38
50	92.71	1.22	-0.46	0.24	1.30	11.06
40	92.50	1.14	-0.44	0.24	1.28	10.06

Table 4-3.Performance and stability results of the baseline 3-stage compressor.

In terms of dynamic stability the compressor stability is relatively high at off-design operating conditions (S_{D40}=1.28) because the compressor design accounts for the shift towards stall in operating incidences of the front stages as operating speed is reduced. However, the more or less uniform level of stability obtained throughout the operating envelope results in a drop in compressor efficiency at high speeds. Consequently, the surge margin per NASA definition had to be set at a value of 11% to ensure that the efficiency at maximum climb conditions remained at adequate levels (η>90%). Given the time constraints of the project, it was not possible to redesign the

baseline compressor to provide a more adequate baseline compressor design with a more suitable operating stability (i.e. SM_{NASA}=20-30%).

Next, the compressor design optimization framework is applied to the baseline compressor to assess whether a better compromise between efficiency at high speeds and operability at design and off-design operating conditions can be reached.

4.4 3-Stage Compressor Design Optimization for Maximum Efficiency

As discussed in Chapter 1, enhancing compressor efficiency has been the objective of many research efforts for the last four decades. To assess the potential impact of the novel compressor design methodology and because it is one of the main concerns in current compressor design practice the first compressor optimization tries to enhance compressor efficiency at high speeds.

First, the objective function and constraints of the compressor optimization are described. Then, the optimized geometry is presented and the design implications of the new methodology are discussed. Finally, the constraint on the operating line pressure ratios is relaxed and the impact on the optimized performance and the design implications are discussed.

4.4.1 Objective Function and Constraints

In order to enhance the compressor efficiency, the objective function used in the compressor optimization of the 3-stage baseline compressor is defined as:

$$\text{Objective} = 0.2\times\left(\frac{\eta_{100}}{\eta_{i100}}\right)+0.5\times\left(\frac{\eta_{90}}{\eta_{i90}}\right)+0.3\times\left(\frac{\eta_{80}}{\eta_{i80}}\right) \tag{4.2}$$

The goal of this optimization effort is to improve the compressor performance throughout the flight envelope with emphasis at cruise, where a low specific fuel consumption is desired. Thus, more weight is given to design conditions compared to maximum climb condition and end of cruise condition. At lower speeds (less than 80%) the improvements in efficiency are less important and thus efficiency at those speeds is not included in the objective function.

In order to guarantee that the results of the blade performance prediction method are accurate the operating incidences need to remain within the admissible range of incidence angles (i.e. i=-6.5° to 12.5°) defined in the blade performance database. In addition, constraints in efficiency and stability are required to ensure that the optimized compressor geometry provides at least the same performance and operability as the baseline compressor geometry throughout the operating envelope. The constraints on the deviation of the operating pressure ratios are summarized in Table 4-4.

Speed	$(\pi-\pi_i)/\pi_i$
100%	± 0.5%
90%	± 0.5%
80%	± 1%
60%	± 1.5%
40%	± 2%

Table 4-4.Operating line constraints used in the compressor design optimization for efficiency.

4.4.2 Optimization Results for Maximum Efficiency

In this section, the performance and the geometry of the compressor optimized for maximum efficiency are presented and compared to the baseline compressor. The results of the compressor design optimization for maximum efficiency are summarized in Table 4-5 and are plotted in Figure 4-3. The original baseline compressor performance is marked by dashed lines and the optimized compressor performance is marked by the solid lines.

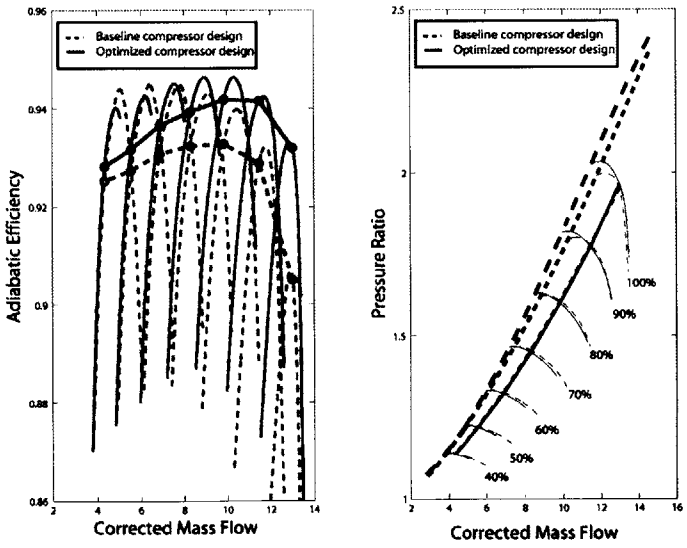

Figure 4-3.Compressor map and efficiency curves for the baseline 3 stage compressor (dashed) and the compressor optimized for maximum efficiency (solid).

SPEED	η (points)	π (%)	σ (%)	R (%)	S_D (%)	SM_{NASA}[2] (points)	SM_{NASA} (%)
100	2.66	0.7%	-18%	-3%	17%	2.97	27
90	1.27	-0.4%	-32%	-43%	45%	4.14	37
80	0.92	-0.5%	-24%	-41%	42%	3.69	33
70	0.69	-0.5%	-17%	-31%	30%	2.99	27
60	0.57	-0.4%	-13%	-14%	15%	2.41	21
50	0.47	-0.3%	-11%	0%	5%	1.99	18
40	0.31	-0.2%	-8%	4%	2%	2.72	27

Table 4-5. Performance improvement results of the compressor design optimization for maximum efficiency.

The compressor efficiency is improved on average by 1% throughout the operating envelope. Note that as illustrated in Figure 4-4 the improvements in efficiency are larger at higher operating speeds as expected from the weighted distribution in the objective function.

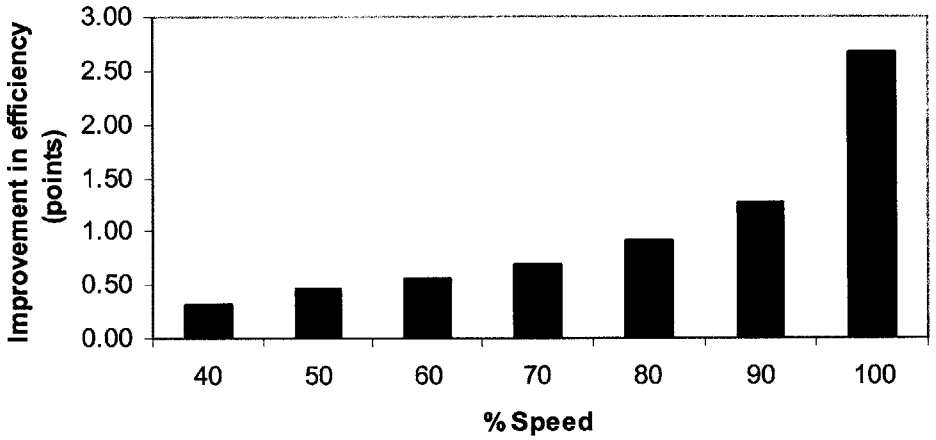

Figure 4-4. % Improvements in efficiency

Additionally, the efficiency of the baseline design at high speeds was compromised to ensure adequate operability at low speeds. This explains the performance improvement of the optimized design at high speeds.

The optimization results also show that the dynamic stability and surge margins are improved even though stability was not explicitly expressed as an objective in the optimization. These improvements are further discussed in next sections.

---

[2] The improvements in surge margin per the industry definition are on the same order of the improvements in surge margin as defined by NASA.

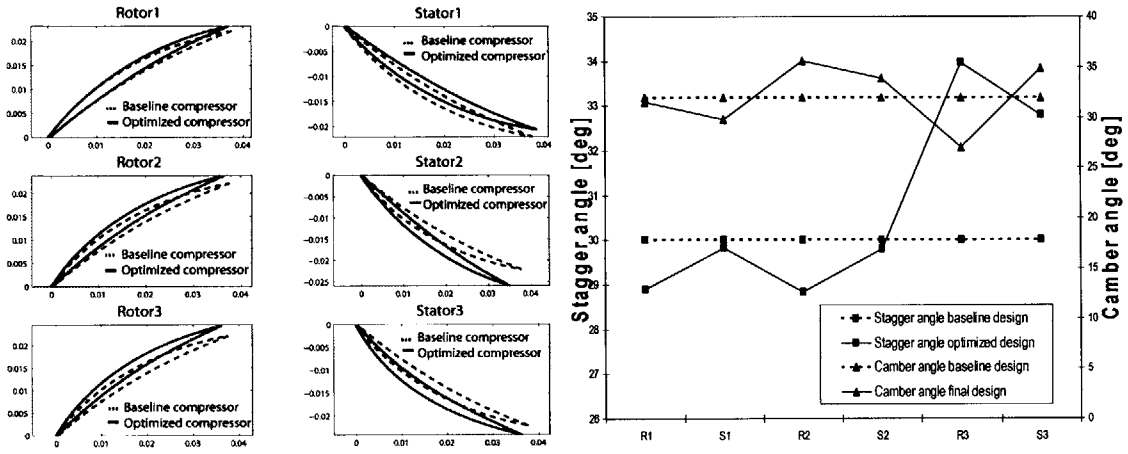

Figure 4-5. Baseline and optimized compressor blade profile configurations (left) and stagger angle and camber angle (right) for the baseline and optimized compressors.

Figure 4-5 illustrates the baseline and optimized compressor configurations and the stagger angle and camber angle of the blade rows for the baseline and the optimized compressor geometries.

The question then arises what the necessary geometric changes are that lead to the above performance improvements.

4.4.3 Design Implications for Maximum Efficiency

Given the problem statement and the assumptions made there are three possible ways to improve the efficiency of the compression system considered. These are reducing the blade-row inlet Mach number, altering the blade row geometry and changing the blade-row inlet flow condition (i.e. incidence). These mechanisms are analyzed next for the optimized compressor to identify the dominating effect responsible for the resulting performance improvement.

	R1		S1		R2		S2		R3		S3	
	Relative Mach number		Relative Mach number		Relative Mach number		Relative Mach number		Relative Mach number		Relative Mach number	
Speed %	Bsl.	Opt.	Bsl.	Opt.	Bsl.	Opt.	Bsl.	Opt.	Bsl.	Opt.	Bsl.	Opt.
100	0.71	0.70	0.68	0.69	0.64	0.64	0.61	0.61	0.58	0.58	0.55	0.53
90	0.61	0.61	0.60	0.60	0.57	0.57	0.54	0.55	0.53	0.53	0.51	0.49
80	0.53	0.52	0.52	0.52	0.50	0.50	0.48	0.49	0.47	0.47	0.46	0.44
70	0.45	0.45	0.45	0.45	0.43	0.44	0.42	0.43	0.42	0.42	0.41	0.39
60	0.38	0.38	0.38	0.38	0.37	0.37	0.36	0.37	0.36	0.36	0.35	0.34
50	0.31	0.31	0.31	0.31	0.31	0.31	0.30	0.31	0.30	0.30	0.30	0.29

Table 4-6. Relative Mach number into the individual blade rows for the baseline and the optimized compressors.

The Mach number impact on loss depends on many variables such as blade thickness, camber and incidence. However, Mach number effects on stagnation pressure loss typically become significant for values larger than 0.7 (Cumpsty [5]). Table 4-6 demonstrates that the changes in relative Mach number between baseline and optimized geometries are low ($M<0.02$) and that the relative Mach numbers throughout the compressor stay below a value of 0.7. This suggests that, Mach number effects are not responsible for the improvements in efficiency observed in the optimized compressor geometry.

The second way to improve the compressor efficiency is to modify the blade row geometry. As discussed in Chapter 3, reducing the stagger angle in a blade row reduces the overall level of loss and thus is a potential source of performance improvement. A comparison between the blade row performance of the baseline and the optimized compressor shows that stator 3 provides the largest improvement in performance. However, Figure 4-5 illustrates that the optimized stator 3 geometry has both a larger stagger angle and camber angle than the baseline stator 3 geometry. Consequently, as shown in Figure 4-6 the average level of loss throughout the range of operating incidences does not diminish. This indicates that changes in blade row geometry to reduce the average level of loss throughout the operating range are not responsible for the improvement in efficiency observed from the optimized compressor geometry.

The third way to enhance compressor performance is to modify the matching of compressor stages. Improving the stage matching for maximum efficiency requires changes in blade incidence angle to values closer to incidence angles that provide minimum loss. This is achieved either by modifying the inlet flow angle or the inlet metal angle of the individual blade rows. A change in inlet flow angle into of a given blade row can be achieved by altering the outlet metal angle of the upstream blade row. Changes in blade row inlet metal angle can be achieved by adjusting the stagger angle and the unstaggered inlet metal angle of the individual blade row. Next, rotor 3 and stator 3 geometric modifications are analyzed. Only, these two blade rows are considered here because they provide the largest performance improvement of the blade rows showing similar trends. The goal is to determine whether the improvement in the

matching of the compressor stages is due to the modification of the inlet flow angles, the inlet metal angles or both.

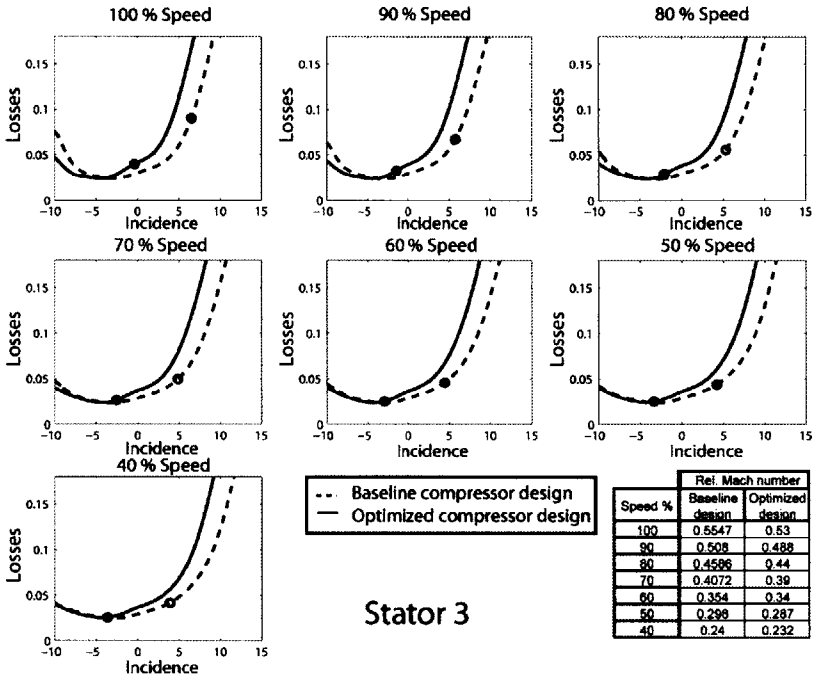

Speed %	Rel. Mach number	
	Baseline design	Optimized design
100	0.5547	0.53
90	0.508	0.488
80	0.4586	0.44
70	0.4072	0.39
60	0.354	0.34
50	0.298	0.287
40	0.24	0.232

Figure 4-6. Loss buckets for stator 3 for the baseline compressor (dashed) and the optimized compressor geometry (solid) at different operating speeds. Working line operating points are marked by circles

Figure 4-6 depicts the loss buckets at different speeds for stator 3 and illustrates the shift in operating incidence to values closer to the incidence at minimum loss. As illustrated in Figure 4-5, camber angle and stagger angle of the third stator blade are both increased. This indicates that the inlet metal angle is increased (+5.655°). In addition, the stagger angle of rotor 3 is increased by 3.974° thus yielding a larger outlet metal angle. The larger outlet flow angle of rotor 3 implies a decrease in inlet flow angle to stator 3(-3.974°). Thus, both the increase in inlet metal angle of the blade row and the increase in outlet metal angle of the blade row upstream are responsible for the improvement in compressor stages matching. For the third stator blade row these changes in geometry result in a total reduction in operating incidence of 9.63°.

The enhanced stability for the optimized compressor at high speeds can be attributed to the improvement in compressor matching. In the baseline case stator 3 is operating at positive incidences on the stall side of the loss bucket at high speeds. The optimization process reduces the operating incidence and shifts the operating points closer to the choke side. This increases the operating range and thus enhances the

overall compressor stability. It can be conjectured that an optimization for maximum efficiency of a baseline compressor that operates close to choke would not provide such improvements in compressor stability. As previously discussed, the compressor optimization framework changes the blade row operating conditions to operating points closer to incidences at minimum loss. For the baseline compressor operating close to choke, these changes require a shift in the operating conditions from negative operating incidences towards positive operating incidences thus reducing the operating range. Consequently, for compressor geometries with choked stages, an optimization for maximum efficiency deteriorates the stability of the compression system.

4.4.4 Effects of Operating Line Constraints on Optimization Results

The constraints on the operating line restrict the design space in which the optimization is conducted. It is important to assess the impact of such a constraint on the optimized compressor performance because one might be willing to accept some fluctuations in operating pressure ratios if a large improvement in efficiency is to be gained. To that avail two different sets of operating line constraints are investigated: in the first set relatively tight constraints are imposed on the operating line. The second set is unconstrained. The two constraint schedules are summarized in Table 4-7.

	Schedule 1	Schedule 2
Speed	$(\pi-\pi_i)/\pi_i$	$(\pi-\pi_i)/\pi_i$
100%	± 0.5%	Unconstrained
90%	± 0.5%	Unconstrained
80%	± 1%	Unconstrained
60%	± 1.5%	Unconstrained
40%	± 2%	Unconstrained

Table 4-7. Two set of constraints used to assess the effect of operating line constrain on optimization results. .

Then, the baseline geometry is optimized for maximum efficiency using the two constraint schedules. Table 4-8, shows the shift in operating line of the optimized compressors for the two operating line constraint schedules 1 and 2.

Operating line constraint π(%) Schedule 1	Operating line shift π(%) Schedule 1	Operating line constraint π(%) Schedule 2	Operating line shift π(%) Schedule 2
±0.5%	0.5%	Unconstrained	-3.4%
±0.5%	-0.5%	Unconstrained	-3.8%
±1%	-0.6%	Unconstrained	-3.2%
±1%	-0.5%	Unconstrained	-2.5%
±1.5%	-0.4%	Unconstrained	-1.9%
±1.5%	-0.3%	Unconstrained	-1.4%
±2%	-0.2%	Unconstrained	-0.9%

Table 4-8. Operating line constraints and operating line shift from baseline pressure ratio values for the two operating line schedules studied.

Table 4-8 illustrates that schedule 1 constraints restrict the search for optimum performance at high speed. This indicates that potentially further efficiency improvements are possible. To asses these potential efficiency enhancements, Figure 4-7 plots the compressor efficiencies for the two optimized compressors.

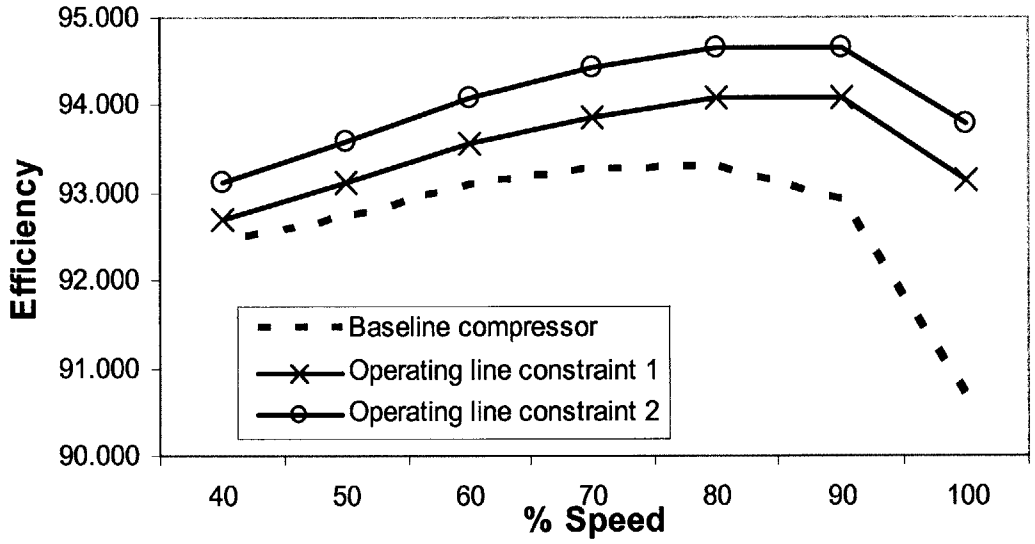

Figure 4-7. Efficiency improvements for both optimized geometries.

An average of 1% efficiency could be gained across the operating envelope if the constraint in pressure ratio on the operating line set by schedule 1 is relaxed. Since the shift in operating line remains low (π<4%) this additional efficiency enhancement is admissible. More importantly it is suggested that the operating line constraint be removed in future optimizations.

4.5 Optimization for Maximum Stability

As discussed in Chapter 1, enhancing compressor operability across the operating envelope is a major focus of current design efforts. The compressor design optimization framework is applied to the 3-stage baseline compressor to investigate the implications of a design for maximum dynamic stability and to assess the potential impact of improvements in compressor matching throughout the operating envelope without the use of bleed valves or variable stator geometries. The objective is to enhance compressor stability and to do so two design philosophies are adopted. The first philosophy optimizes for maximum dynamic stability at cruise while the second philosophy also includes an stability objective at idle speed. First, the objective functions and constraints of the two compressor optimizations are described. Then, the optimized geometries are presented and the design implications of the new methodology are discussed.

4.5.1 Objectives Functions and Constraints

In order to enhance compressor stability, two objective functions are used in the compressor optimizations for maximum stability of the 3 stage baseline compressor:

$$\text{OBJ1} = \frac{1}{3}\times\left(\frac{S_{D100}}{S_{Di100}}\right)+\frac{2}{3}\times\left(\frac{S_{D70}}{S_{Di70}}\right) \tag{4.3}$$

$$\text{OBJ2} = \frac{1}{4}\times\left(\frac{S_{D100}}{S_{Di100}}\right)+\frac{1}{2}\times\left(\frac{S_{D90}}{S_{Di90}}\right)+\frac{1}{4}\times\left(\frac{S_{D40}}{S_{Di40}}\right) \tag{4.4}$$

The goal of the first design optimization philosophy (Equation (4.3)) is to improve the compressor stability at maximum climb conditions and at end of cruise conditions. This will be compared to the second design philosophy for enhanced operability which is aimed at improving the compressor stability at maximum climb conditions, design conditions and also at idle conditions where engine accelerations and low flow coefficients can trigger instability.

The constraints used in both compressor design optimization problems are identical and are the same as used in the compressor design optimization for maximum efficiency. These constraints are the incidence bounds on the operating

incidences of the different blade rows, the minimum requirements in efficiency and stability across the compressor map and the constraints on the compressor operating pressure ratios summarized in Table 4-4.

4.5.2 Optimization Results for Maximum Stability

Using the above discussed objectives and constraints the compressor design optimization framework was executed. The results of the optimization for maximum dynamic stability are summarized in Table 4-9.

	η (points)		π (%)		σ (%)		R (%)		S_D (%)		SM_{NASA} (points)		SM_{NASA} (%)	
SPD (%)	Obj. 1	Obj. 2	Obj. 1	Obj. 2	Obj. 1	Obj. 2	Obj. 1	Obj. 2	Obj. 1	Obj. 2	Obj. 1	Obj. 2	Obj. 1	Obj. 2
100	2.2	1.6	0.6%	0.7%	-20%	-23%	-36%	5%	24%	20%	4.4	3.2	40	29
90	1.3	0.7	-0.4%	-0.4%	-38%	-30%	-30%	-12%	39%	25%	4.9	3.5	44	31
80	0.8	0.5	-0.8%	-0.8%	-31%	-26%	-34%	-13%	40%	21%	4.6	3.2	41	29
70	0.5	0.4	-0.9%	-0.8%	-24%	-18%	-28%	-5%	31%	12%	4.0	2.9	35	26
60	0.4	0.2	-0.8%	-0.7%	-20%	-14%	-12%	1%	17%	6%	3.5	2.9	31	25
50	0.3	0.1	-0.6%	-0.6%	-16%	-11%	0%	5%	7%	3%	3.3	2.8	29	26
40	0.1	0.0	-0.4%	-0.4%	-14%	-11%	1%	-6%	6%	8%	3.7	3.5	36	35

Table 4-9.Results of the two compressor design optimizations for maximum stability.

Figure 4-8 illustrates the distribution of the new stability metric S_D as a function of operating speed for the baseline and the optimized compressors using the two stability based objective functions. The compressor optimized for maximum stability using objective 1 shows a larger improvement in stability over the entire speed range except at 40% speed. The compressor design optimized based on objective 2 is more stable compared to the baseline compressor but on average is less stable than the compressor design optimized with objective 1.

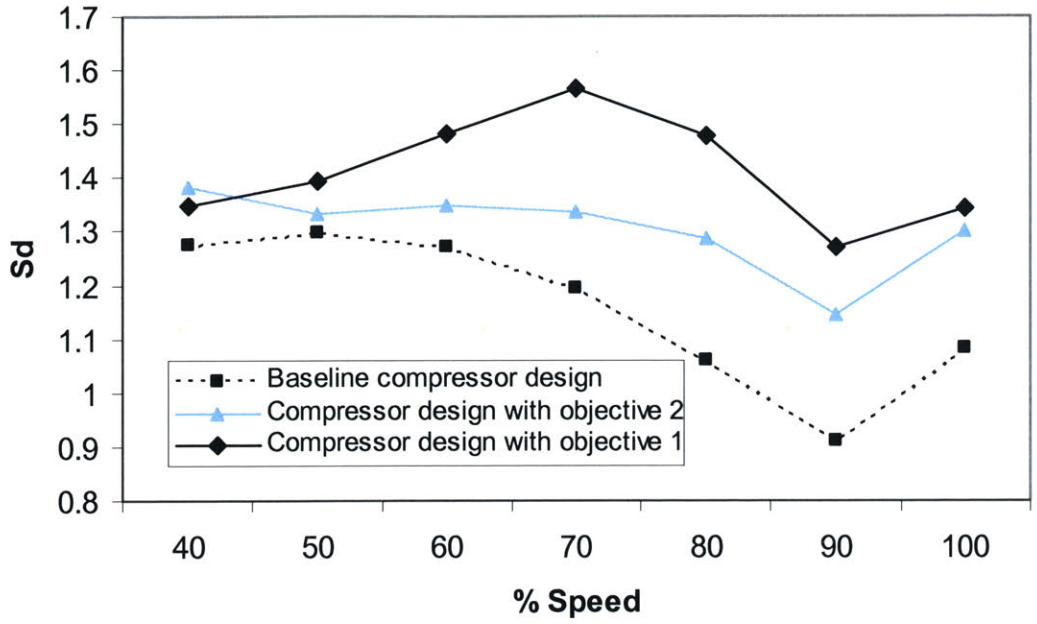

Figure 4-8. New stability metric S_D for the baseline compressor design and the two compressor designs optimized for maximum stability.

Given the objectives of the two optimizations the results are as expected from the given stability objectives. Furthermore, the results indicate that including an stability objective at end of cruise conditions yields better stability results than including an stability objective at idle conditions.

It is worthwhile analyzing the effect of the stability based optimization on compressor efficiency. Table 4-9 indicates that optimizing for enhanced stability enhances compressor efficiency in both optimizations by an average of η=0.8% (objective 1) and η=0.5% (objective 2). The source of these improvements is further discussed in next sections.

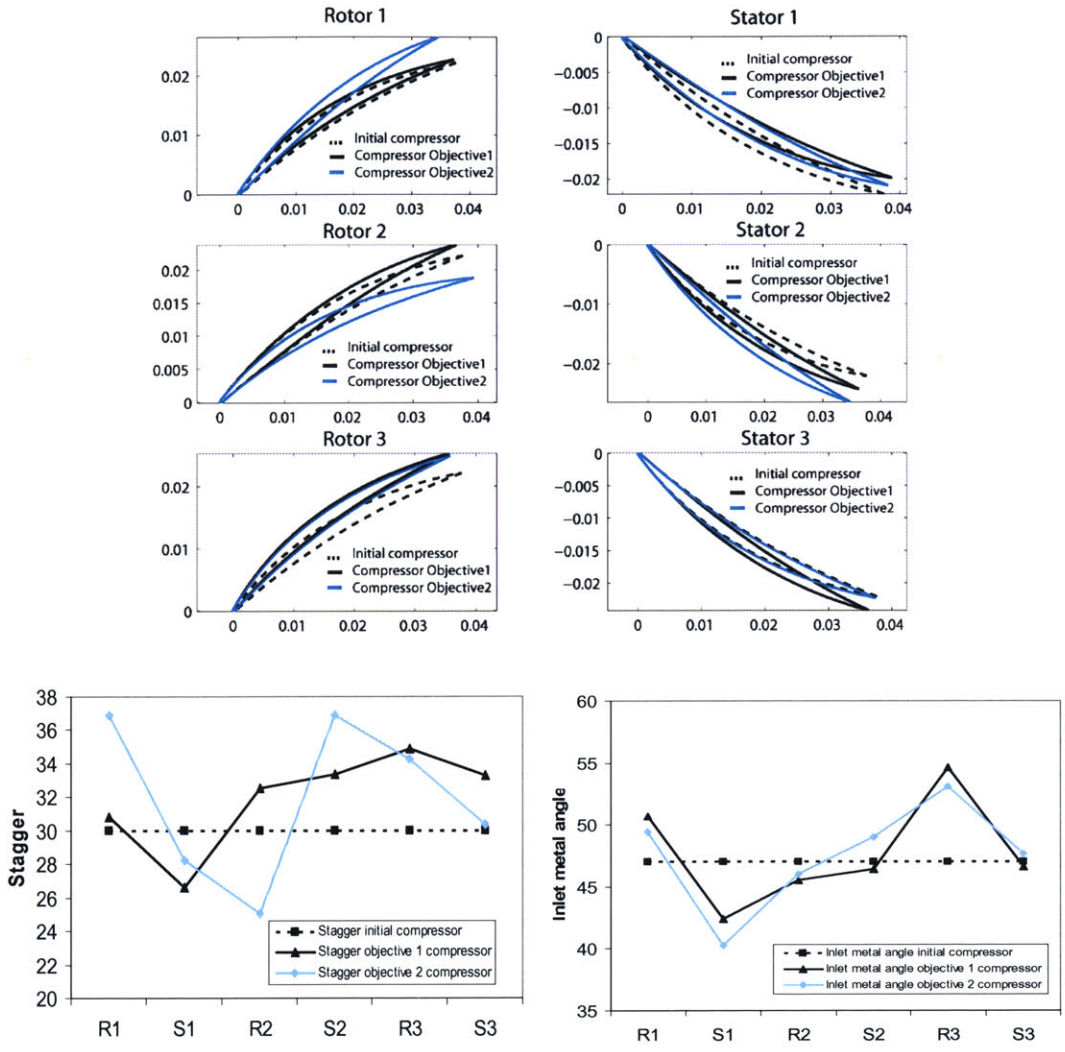

Figure 4-9. Blade profiles (top), stagger angle (left) and camber angle (right) for the baseline compressor design and the two compressor designs optimized for maximum stability.

Figure 4-9 illustrates the baseline and optimized compressor configurations and the stagger angle and camber angle of the individual blade rows for the baseline and the two optimized compressor geometries. These are used in the next sections to assess the design implications of the optimizations for enhanced dynamic stability.

4.5.3 Design Implications for Maximum Stability

This section presents a simplified analysis to identify the mechanisms responsible for the improvements in dynamic stability. Then, the results of the compressor design optimizations for maximum stability are analyzed to identify which

of these mechanisms is responsible for the enhanced stability of the resulting compressor designs.

The improvements in dynamic stability captured by the new metric S_D of both compressor design optimizations can essentially be related to changes in the growth rate of the perturbations in the flow field since σ carries twice the weight of the robustness R in S_D. The Moore-Greitzer dynamic stability model predicts that $\sigma \propto \frac{\partial \psi_{ts}}{\partial \phi}$ where the non-dimensional total-to-total pressure rise of an individual blade row can be expressed as follows:

$$\psi_{tt} = \phi \times (\tan \alpha_1 - \tan \alpha_2) - L \tag{4.5}$$

Differentiating the above with respect to flow coefficient and neglecting the dynamic head at the exit of the blade row one can write:

$$\sigma \propto \left(\tan(\alpha_1) - \tan(\alpha_2)\right) - \frac{\partial L}{\partial \phi} \tag{4.6}$$

This implies that the flow turning (related to blade geometry) and performance of the blade row govern the dynamic stability σ. Since the exit flow angle is constant throughout the compressor design optimization, an improvement in stability (decrease in σ) is obtained either by decreasing α_1 or by increasing the stagnation pressure loss sensitivity $\partial L / \partial \phi$. Increasing $\partial L / \partial \phi$ is achieved by altering the compressor stages matching to operate with higher flow coefficients (negative incidences) or by changing the shape of the blade row loss characteristic.

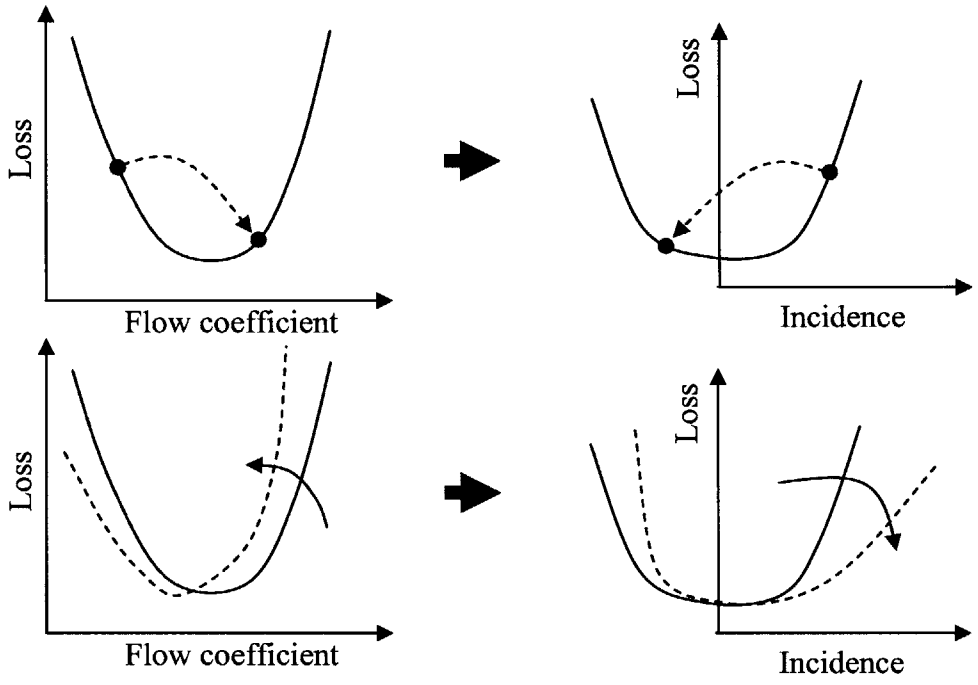

Figure 4-10. Schematic enhancing dynamic stability by increasing $\partial L/\partial \phi$ through changes in compressor stages matching (top) or by changing the shape of the blade row loss characteristic (bottom).

Figure 4-10 (top) illustrates schematically that in order to enhance σ through a increase in $\partial L/\partial \phi$, the operating point has to move to higher flow coefficients. This operating condition at higher flow coefficient indicates that incidence angles must be decreased. As discussed in previous sections, a decrease in incidence is obtained either by increasing the exit metal angle of the preceding blade row or by increasing the inlet metal angle into the blade row considered. Figure 4-10 (bottom) shows the effect of changing the shape of the blade row loss characteristic on the improvement of dynamic stability. It is desired to have a reduced slope on the positive incidence side while on the negative incidence side an increase in slope to maximize $\partial L/\partial \phi$ is wanted. As discussed in Chapter 3, this modification in loss bucket shape is obtained by decreasing the camber angle of the individual blade rows. Since improving the compressor stage matching requires larger inlet metal angles and changing the shape of the blade row loss characteristic requires lower inlet metal angles, the two objectives are in conflict and a compromise must be made.

Next, the results of the compressor optimizations for enhanced stability are analyzed to elucidate which of the two effects, matching the compressor stages or changing of the loss bucket shape, dominate the compressor design optimizations for maximum stability. The geometric modifications to stator 3 are studied because it is the blade row that provides the largest stability improvements. Figure 4-11 presents stator 3 loss buckets at different speeds for the baseline compressor design and the optimized compressor design based on objective 1. Both a reduction in incidence angle and a change in blade row loss characteristic are observed. In addition, Figure 4-9 shows that stator 3 inlet metal angle is unaltered. This indicates that none of the two possible geometric changes (change in loss bucket and matching) dominate the compressor design optimization for maximum stability. The decrease in incidence to improve the stage matching is the result of a decrease in the inlet flow angle into stator 3 driven by a larger rotor 3 stagger angle. The stabilization of the blade row is the result of a decrease in stator 3 camber angle while the inlet metal angle is kept unaltered even though the stator 3 stagger angle is increased.

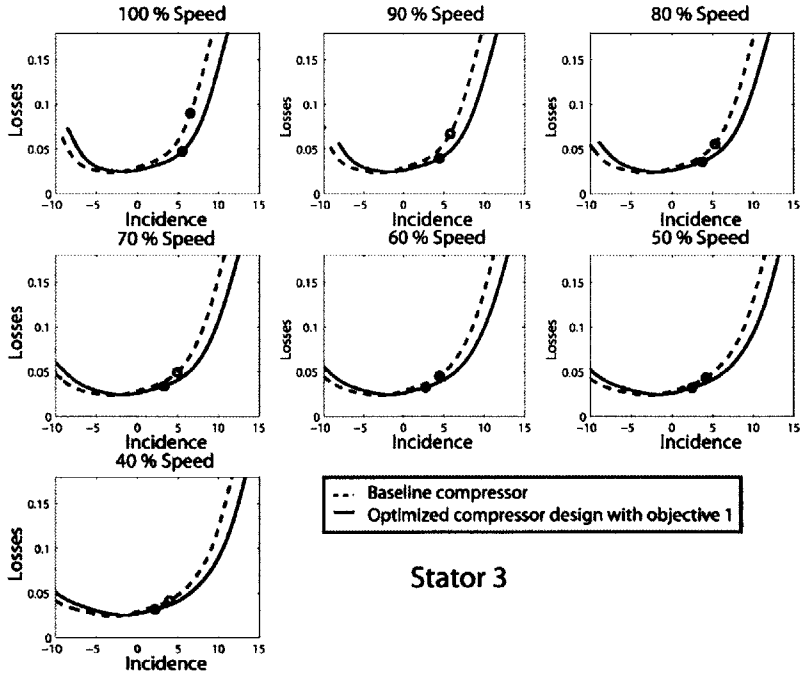

Figure 4-11. Loss buckets for stator 3 for the baseline compressor and the optimized compressor for maximum stability using objective 1.

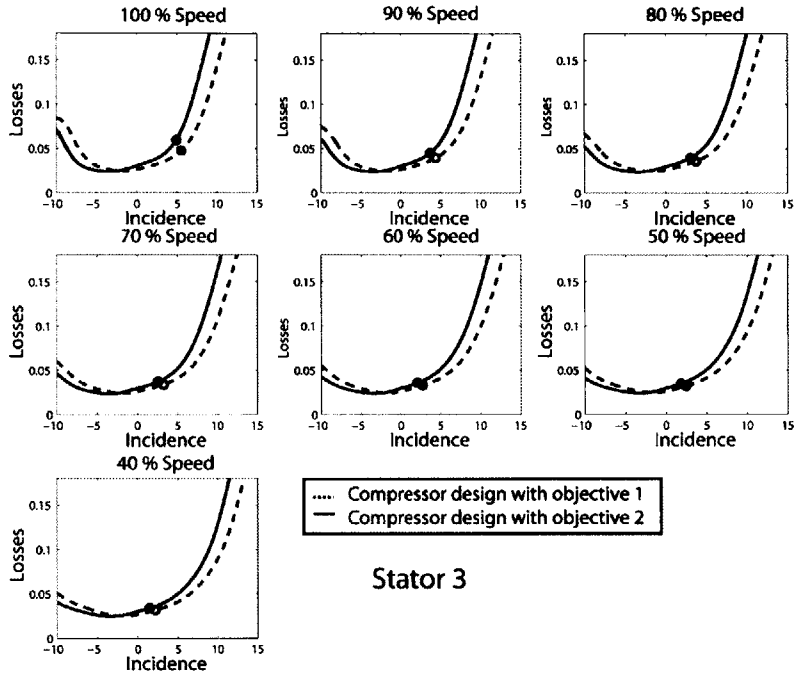

Figure 4-12. Loss buckets for stator 3 for the optimized compressor for maximum stability using objectives 1 and 2.

Figure 4-12, compares the stator 3 loss characteristics at different operating speeds for the optimized geometries using objectives 1 and 2. Since the optimized stator 3 based on objective 2 and the baseline stator 3 yield very similar loss buckets, the baseline loss characteristics were omitted in Figure 4-12 for clarity. While the matching of the two optimized compressors is similar, the compressor design optimized based on objective 1 presents a more stable blade row due its lower loss sensitivity on the positive incidence side. This is the result of the lower camber angle of stator 3 for the compressor design based on objective 1 (φ=-4°).

The improvements in efficiency observed in both optimizations are caused by changes in compressor stage matching and shifts in the loss buckets for blade rows operating at positive incidence in the baseline compressor. If a blade row is operating at positive incidence angle a change in the stage matching to improve stability diminishes the incidence angle to values closer to incidence at minimum loss. The change in the shape of the loss bucket decreases the loss on the positive incidence side and yields a performance improvement. On the other hand, if the blade row is operating at a negative incidence the improvement in the matching of the compressor stages for maximum

stability and the stabilization of the blade rows further increase the losses and deteriorate the efficiency of the compressor.

4.6 Summary

The compressor design optimization framework implemented for a 3 stage compressor has been implemented for two different design philosophies. The first philosophy consists in enhancing compressor efficiency at high speeds and the second to improve the compressor dynamic stability throughout the operating envelope.

The compressor design optimization for maximum efficiency indicates that the main mechanism behind the enhancement in compressor efficiency is to adjust the stage matching in order to operate at incidence angle near minimum loss. If an individual blade row is close to stall the optimizer reduces the operating incidence to values closer to incidence at minimum loss. If on the other hand an individual blade row is close to choke the opposite occurs. The changes in operating incidences are the result of modifications to the inlet metal angle of the blade row considered and the outlet metal angle of the preceding blade row. The results of the compressor design optimization for enhanced efficiency are encouraging since an average increase in efficiency of 1% is obtained across the operating envelope and a 2.7% enhancement of efficiency is obtained at maximum climb condition. Further, the optimization for enhanced efficiency also provides an improvement in stability with an average gain in surge margin per NASA definition of 3 points throughout the working line.

The second design philosophy aimed at improving dynamic stability across the compressor map. The results of the compressor design optimizations for maximum stability indicate that there are two mechanisms to enhance compressor stability. The first mechanism is governed by changes in stages matching to operate at lower incidences. This is achieved by decreasing the inlet flow angle while keeping the inlet metal angle constant. The second mechanism to enhance dynamic stability is related to changes in the loss sensitivities which can be achieved through decreases in blade row camber. The results of this second approach are also promising since dynamic stability is shown to be improved by 23% and surge margin as defined in industry by 3.8 points throughout the operating envelope.

The three compressor optimization case studies carried out in this thesis clearly illustrate the impact of the different design philosophy on the compressor blade row geometry since the three yield three different compressor architectures.

Chapter 5

Summary and Conclusions

This thesis introduces a new way to quantify the stability of compression systems. Unlike surge margin, the new metric is directly related to the damping of the natural oscillations of the compression system that lead to rotating stall and surge. Furthermore, the new metric captures the shape of the compressor characteristic such that it accounts for the sensitivity of compressor stability to changes in operating line conditions. This metric is used as a primary design variable in a compressor optimization design framework with the goal to enhance compressor performance and operability. The novel design methodology is applied to a generic three repeating stage axial compressor. The baseline three-stage compressor design is optimized to demonstrate the potential performance and operability improvements. More specifically, the work presented in this thesis addressed the following objectives:

5.1 Assessment of the Shortcomings of Surge Margin

Surge margin is the commonly used metric to quantify the stability of a compression system. There are two definitions used in practice: the first definition quantifies the margin in pressure ratio between surge point and operating point at constant corrected mass flow whereas the second definition considers the change in outlet corrected flow between the operating point and the surge point for the same corrected rotational speed.

Both definitions are currently in use to guarantee that instabilities are avoided throughout the compressor operating envelope. The rotating stall and surge instabilities are the mature forms of the natural oscillations of small perturbations in the flow field, and the damping of these oscillations is directly related to the slope of the compressor

characteristics. To contrast the surge margin metrics with the actual damping ratios of the flow field oscillations, the stability of a three-stage compressor is quantified by the two surge-margin definitions and by computing the changes in damping ratio along the operating line. The results indicate that there is no correlation between the three stability assessment methods and that the changes in damping ratio along the operating line much more fundamentally represent the dynamic behavior and stability margin of the compression system. Furthermore it is noted that, in comparison, surge margin is a more conservative measure of stability and it is conjectured that a stability metric based on dynamic considerations could potentially enable compressor designs with enhanced performance.

5.2 Development of a New Stability Metric Based on Dynamic Considerations

Based on the comparison between surge margin and the damping ratio of the natural flow field oscillations a new stability metric is developed. The dynamic compressor stability metric is comprised of two parts. In the first part, the dynamic behavior of the compression system at operating conditions is captured by quantifying the growth rate of the perturbations in the flow field. As predicted by the Moore-Greitzer [19] theory this quantity depends on the slope of the non-dimensional total-to-static pressure rise characteristic and thus is closely related to the compressor blade rows loss characteristics. The second part of the new stability metric quantifies the deterioration in the compressor dynamic stability with changes in working condition and is referred to as robustness of dynamic stability to changes in operating conditions. To illustrate the importance of this attribute of the new stability metric an example is used where the relation between the shape of the non-dimensional pressure rise characteristic and the robustness is demonstrated. In order to capture the entire shape of the pressure rise characteristic, robustness is defined as the geometric mean of the local curvatures of the pressure rise characteristic in the operating range of interest. The new stability metric is then defined as a compound of both attributes. Weighting factors can be assigned to each of the attributes in order to capture different operability requirements. Next, the surge margin and the new stability metric are computed for a

three-stage baseline compressor to assess the benefits of the new metric. The results show that the surge margin per the industry definition does not correlate with the new metric and that surge margin as defined by NASA can qualitatively capture some of the dynamic stability trends. However, only the new stability metric is able to quantify the dynamic behavior of the compression system and is thus suggested to be used as a prime design variable in the novel compressor design optimization framework.

5.3 Implementation of the New Stability Metric in a Compressor Design Optimization Framework

A new compressor design optimization framework is implemented based on the previous effort by Perrot [20]. The optimization allows a versatile definition of the objective function such that any combination of pressure ratio, efficiency and dynamic stability can be prescribed. Furthermore, the final objective function can include individual objectives at various operating speeds. This is a key feature which allows to achieve the best possible compromise between objective functions at design and off-design operating conditions.

The compressor design optimization framework uses an effective blade-to-blade CFD method (fast blade performance prediction method) to predict the blade row performance which is used to evaluate the compressor performance and dynamic stability. The fast blade performance prediction method consists of an N-dimensional interpolation method in conjunction with a blade performance database that is generated using MISES. The method enables to estimate the blade performance in dependence of a number of user defined geometric blade parameters. The fast blade performance prediction method is estimated to be 100 times faster than a direct numerical simulation and it is shown that the accuracy is within 2% of the direct numerical simulation results.

5.4 Application of the Compressor Design Optimization Framework to a Generic Three Stage Compressor

One of the key objectives of this research is to apply the novel compressor design methodology to the three-stage baseline compressor. To assess the potential

benefits of adopting this methodology in the design phase, two different design philosophies commonly used in compressor design practice were adopted.

The first design philosophy used in the optimization is aimed at improving efficiency, especially at operating speeds where a low specific fuel consumption is desired.

The second optimization design philosophy implemented in the compressor design framework is targeted to improve operability over the entire compressor operating range without variable stator geometry and inter-stage bleed valves as it is often the case for low pressure compressors. Such a compressor design optimization could potentially reduce the complexity of the compressor architecture and increase the thrust-to-weight ratio.

5.5 Demonstration of Performance and Operability Enhancements using the Novel Compressor Design Methodology

To demonstrate the potential performance improvements using the compressor design optimization framework the two design philosophies are implemented. The major goal is to enhance the compressor efficiencies at high speed and to improve the operability throughout the operating envelope.

The results of the compressor design optimization for enhanced efficiency demonstrate that improvements in efficiency are due to an optimal matching of the compressor stages. The optimum stage matching which entails incidence angles close to minimum loss conditions is achieved through changes in the blade row inlet and exit metal angles. The results of the compressor design optimization for maximum efficiency are promising: an average efficiency improvement of 1% is obtained throughout the operating envelope, and at maximum climb conditions an efficiency enhancement of 2.7% is achieved. Furthermore, optimizing for efficiency does not deteriorate stability but yields an average improvement in surge margin per the industry definition of 2.6 points along the working line. In addition, the impact of the operating line constraints on optimized compressor performance was assessed. It is demonstrated

that an additional 1% efficiency improvement can be obtained if the pressure ratio variations along the operating line are allowed to vary by 4%.

The compressor design optimization based on enhanced dynamic stability provides on average a 23% improvement in the newly developed stability metric which translates into a surge margin enhancement of 4 points on average across the entire compressor map. The dynamic stability enhancements are the result of improvements in compressor stage matching and of modifications in the loss buckets due to geometric changes in the blade profiles. An improvement in compressor matching for enhanced dynamic stability demands incidence angle changes which can be achieved through changes in the outlet metal angle of the preceding blade rows and by decreasing the camber angle. Furthermore it is observed that the compressor design optimization for enhanced dynamic stability also implies improvements in compressor efficiency although the optimization objective does not explicitly account for efficiency improvements. In particular, for the cases investigated, the compressor efficiency was improved by an average of 0.65 points throughout the operating envelope.

5.6 Recommendations for Future Work

The research effort presented in this thesis constitutes the definition of a new compressor stability metric and a proof-of-concept study of a novel compressor design optimization method. To achieve these goals within the timeframe of this thesis many assumptions had to be made. Based on these and the outcomes of this research, the following recommendations can be made for future work.

The mean-line flow solver and the dynamic model assume two-dimensional flow and thus neglect three-dimensional effects such as endwall losses and hub corner stall. These three-dimensional loss effects are important in advanced compressor designs and should be included in the optimization framework. Furthermore the fast blade prediction method should be extended to predict blade deviation angles in order to replace the empirical correlations currently used in the framework.

Alternative CFD flow solvers are envisaged in the fast blade performance prediction method to enable the performance assessment of a broader range of blade geometries and flow conditions: in particular very large stagger angles, camber angle

and higher Mach numbers (transonic conditions). Moreover, the blade performance database can be readily extended to more than two geometric variables used in this thesis. This would yield further degrees of freedom in the optimization process and potentially enable even larger performance and operability enhancements.

In summary, the outcomes of this thesis are encouraging and it is suggested to apply the developed optimization framework and novel stability metric to an industrial strength problem to assess the capabilities in a real compressor environment.

Appendix A

Description of Blade Row Losses and Dynamics

This appendix describes the approach adopted to evaluate the sensitivities of blade row loss to changes in flow inlet conditions and presents the modifications to the transmission matrices in the rotating stall inception prediction model. The ducts in the model are considered inviscid and hence no changes to the transmission matrices of these components are required (for information on the derivation of the transmission matrices of ducts/gaps refer to Spakovszky [24]).

A.1 Losses

The sole sources of blade row losses included in the calculations throughout this thesis are blade profile losses. These are calculated using blade-to-blade CFD (MISES or blade performance prediction method) and are represented by the loss coefficient $\omega = \frac{\Delta p_t}{p_{t1} - p_1}$. The dynamic compressor model requires a slightly different description of the blade row losses, namely $L = \frac{\Delta p_t}{\rho U^2}$ and thus the resulting loss coefficients obtained from CFD need to be modified before introducing them into the dynamic compressor model. Assuming incompressible flow, the two definitions are related according to:

$$L = \tfrac{1}{2}\left(\frac{V}{U}\right)^2 \omega$$

Due to the difficulty in experimentally of measuring flow angles the dependence of loss coefficient with incidence is generally not available. Instead, the dependence of

loss coefficient with flow coefficient, (which is readily measured), was used to calculate the required losses sensitivities for the dynamic model (Moore Greitzer [17], Spakovszky [25]).

The information on blade performance gathered from CFD allows an accurate description of the loss coefficient with incidence and thus the previously discussed assumption is not required. This demands a modification of the loss derivatives and transmission matrices previously used. If inlet axial and tangential velocities are independent, the losses need to be rewritten as a function of V_{x1} and $V_{\theta 1}$ and derived accordingly:

$$\text{Rotor: } L = \frac{1}{2}\left(\frac{V_{x1}^2 + (U - V_{\theta 1})^2}{U^2}\right)\omega(i)$$

$$\text{Stator: } L = \frac{1}{2}\left(\frac{V_{x1}^2 + V_{\theta 1}^2}{U^2}\right)\omega(i)$$

Where the loss coefficient $\omega(i)$ obtained from the blade-to-blade CFD analysis is only a function of incidence.

After differentiation, the loss derivatives with respect to V_{x1} and $V_{\theta 1}$ yield for the stator:

$$\frac{\partial L_S^{ss}}{\partial V_{x1}} = \frac{\partial}{\partial V_{x1}}\left[\frac{1}{2}\left(\frac{V_{x1}^2 + V_{\theta 1}^2}{U^2}\right)\right]\omega(i) + \frac{1}{2}\left(\frac{V_{x1}^2 + V_{\theta 1}^2}{U^2}\right)\frac{\partial \omega(i)}{\partial i}\frac{\partial i}{\partial V_{x1}}$$

$$\frac{\partial L_S^{ss}}{\partial V_{x1}} = \frac{V_{x1}}{U}\omega(i) - \frac{V_{\theta 1}}{2U}\frac{\partial \omega(i)}{\partial i}$$

$$\frac{\partial L_S^{ss}}{\partial V_{\theta 1}} = \frac{\partial}{\partial V_{\theta 1}}\left[\frac{1}{2}\left(\frac{V_{x1}^2 + V_{\theta 1}^2}{U^2}\right)\right]\omega(i) + \frac{1}{2}\left(\frac{V_{x1}^2 + V_{\theta 1}^2}{U^2}\right)\frac{\partial \omega(i)}{\partial i}\frac{\partial i}{\partial V_{\theta 1}}$$

$$\frac{\partial L_S^{ss}}{\partial V_{\theta 1}} = \frac{V_{\theta 1}}{U}\omega(i) + \frac{V_{x1}}{2U}\frac{\partial \omega(i)}{\partial i}$$

Similarly, the loss derivatives with respect to V_{x1} and $V_{\theta 1}$ for the rotor become:

$$\frac{\partial L_S^{ss}}{\partial V_{x1}} = \frac{\partial}{\partial V_{x1}}\left[\frac{1}{2}\left(\frac{V_{x1}^2 + (U - V_{\theta 1})^2}{U^2}\right)\right]\omega(i) + \frac{1}{2}\left(\frac{V_{x1}^2 + (U - V_{\theta 1})^2}{U^2}\right)\frac{\partial \omega(i)}{\partial i}\frac{\partial i}{\partial V_{x1}}$$

$$\frac{\partial L_R^{ss}}{\partial V_{x1}} = \frac{V_{x1}}{U}\omega(i) + \frac{(V_{\theta 1} - U)}{2U}\frac{\partial \omega(i)}{\partial i}$$

$$\frac{\partial L_R^{ss}}{\partial V_{\theta 1}} = \frac{\partial}{\partial V_{\theta 1}}\left[\frac{1}{2}\left(\frac{V_{x1}^2 + (U - V_{\theta 1})^2}{U^2}\right)\right]\omega(i) + \frac{1}{2}\left(\frac{V_{x1}^2 + (U - V_{\theta 1})^2}{U^2}\right)\frac{\partial \omega(i)}{\partial i}\frac{\partial i}{\partial V_{\theta 1}}$$

$$\frac{\partial L_R^{ss}}{\partial V_{\theta 1}} = \frac{(V_{\theta 1} - U)}{U}\omega(i) - \frac{V_{x1}}{2U}\frac{\partial \omega(i)}{\partial i}$$

A.2 Rotor/Stator Transmission Matrices

The availability of the two loss derivatives requires some minor modifications to the transmission matrices for the rotor and stator blade row components. Below, the governing equations for each of the modules are linearized and the new matrices are rewritten following the procedure outlined in Spakovszky [24]. The following matching conditions hold in non-dimensional form across the rotor and stator semi-actuator disks for the rotor:

$$V_{x1} = V_{x2}$$

$$V_{\theta 2} = 1 + V_{x2}\tan\beta_2$$

$$P_{t2} - P_{t1} = 1 + (\tan\beta_2 - \tan\alpha_1)V_{x1} - \lambda_{rot}\left(\frac{\partial V_{x1}}{\partial \tau} + \frac{\partial V_{x1}}{\partial \theta}\right) - L_R$$

$$(1 + \tau_R\left[\frac{\partial}{\partial \tau} + \frac{\partial}{\partial \theta}\right])L_R = L_R^{ss}(V_{x1}, V_{\theta 1})$$

and for the stator:

$$V_{x1} = V_{x2}$$

$$V_{\theta 2} = V_{x2}\tan\alpha_2$$

$$P_{t2} - P_{t1} = -\lambda_{sta}\left(\frac{\partial V_{x1}}{\partial \tau}\right) - L_S$$

$$(1 + \tau_S\frac{\partial}{\partial \tau})L_R = L_S^{ss}(V_{x1}, V_{\theta 1})$$

Linearizing and taking the Laplace transform for the n-th harmonic, the flow field perturbation becomes for the rotor:

$$\tilde{V}_{x1,n} = \tilde{V}_{x2,n}$$

$$\tilde{V}_{\theta 2,n} = \tilde{V}_{x2,n}\tan\beta_2$$

$$\widetilde{P}_{2,n} + \overline{V}_{\theta 2}\widetilde{V}_{\theta 2,n} - \widetilde{P}_{1,n} - \overline{V}_{\theta 1}\widetilde{V}_{\theta 1,n} =$$

$$(\tan\beta_2 - \tan\alpha_1 - \lambda_{rot}(s+jn))\widetilde{V}_{x1,n} - \left(\frac{\partial L_R^{ss}}{\partial V_{x1}}\widetilde{V}_{x1,n} + \frac{\partial L_R^{ss}}{\partial V_{\theta 1}}\widetilde{V}_{\theta 1,n}\right)\frac{1}{(1+\tau_R(s+jn))}$$

and for the stator:

$$\widetilde{V}_{x1,n} = \widetilde{V}_{x2,n}$$

$$\widetilde{V}_{\theta 2,n} = \widetilde{V}_{x2,n}\tan\alpha_2$$

$$\widetilde{P}_{2,n} + \overline{V}_{\theta 2}\widetilde{V}_{\theta 2,n} - \widetilde{P}_{1,n} - \overline{V}_{\theta 1}\widetilde{V}_{\theta 1,n} = (-\lambda_{sta}s)\widetilde{V}_{x1,n} - \left(\frac{\partial L_S^{ss}}{\partial V_{x1}}\widetilde{V}_{x1,n} + \frac{\partial L_S^{ss}}{\partial V_{\theta 1}}\widetilde{V}_{\theta 1,n}\right)\frac{1}{(1+\tau_S s)}$$

For each harmonic the above matching conditions can be written in matrix form to relate the perturbations upstream and downstream of each semi-actuator disk. Summing up the transmission matrices over all harmonics, the downstream flow field perturbations can be calculated from the upstream perturbations according to:

$$\begin{bmatrix} \partial V_{x2} \\ \partial V_{\theta 2} \\ \partial P_2 \end{bmatrix}(\theta, s) = \sum_{n=0}^{\infty} \mathrm{B}_{Rot,n} \begin{bmatrix} \widetilde{V}_{x1} \\ \widetilde{V}_{\theta 1} \\ \widetilde{P}_1 \end{bmatrix}_n (s)$$

for the rotor and :

$$\begin{bmatrix} \partial V_{x2} \\ \partial V_{\theta 2} \\ \partial P_2 \end{bmatrix}(\theta, s) = \sum_{n=0}^{\infty} \mathrm{B}_{Sta,n} \begin{bmatrix} \widetilde{V}_{x1} \\ \widetilde{V}_{\theta 1} \\ \widetilde{P}_1 \end{bmatrix}_n (s)$$

for stator where the transmission matrices for the blade rows are defined as:

$$\mathrm{B}_{Rot,n} = \begin{bmatrix} 1 & 0 & 0 \\ \tan\beta_2 & 0 & 0 \\ \left[\tan\beta_2 - \tan\alpha_1 - \lambda_{rot}(s+jn) - \overline{V}_{\theta 2}\tan\beta_2\right] & \overline{V}_{\theta 1} - \dfrac{\partial L_R^{ss}}{\partial V_{\theta 1}}\dfrac{1}{(1+\tau_R(s+jn))} & 1 \\ \left[-\dfrac{\partial L_R^{ss}}{\partial V_{x1}}\dfrac{1}{(1+\tau_R(s+jn))}\right] & & \end{bmatrix} e^{jn\theta},$$

and

$$\mathrm{B}_{Sta,n} = \begin{bmatrix} 1 & 0 & 0 \\ \tan\alpha_2 & 0 & 0 \\ \left[-\lambda_{sta}s - \overline{V}_{\theta 2}\tan\beta_2 - \dfrac{\partial L_S^{ss}}{\partial V_{x1}}\dfrac{1}{(1+\tau_S s)}\right] & \overline{V}_{\theta 1} - \dfrac{\partial L_S^{ss}}{\partial V_{\theta 1}}\dfrac{1}{(1+\tau_S S)} & 1 \end{bmatrix} e^{jn\theta}.$$

Bibliography

[1] BLANVILLAIN, E., "*Dynamic Stability Analysis of a Multi-Stage Axial Compressor with Design Implications*". Master's Thesis, Department of Aeronautics and Astronautics, Massachusetts Institute of Technology, Feb. 2003.

[2] BONNAURE, L.P.,"*Modelling High Speed Multistage Compressor Stability*". Master's thesis, Massachusetts Institute of Technology, 1991.

[3] BUCHE, D., GUIDATI, G., STOLL, P.,"*Automated Design Optimization of Compressor Blades for Stationary, Large-Scale Turbomachinery*". GT2003-38421. Proceedings of the ASMA Turbo Expo 2003.

[4] CAMP,T.R., DAY, I.J.,"*A Study of Spike and Modal Stall Phenomena in a Low-Speed Axial Compressor*". Journal of Turbomachinery, Transactions of the ASME, Vol. 120 (1998), pp. 393-401.

[5] CUMPSTY, N., "*Compressor Aerodynamics*". Addison-Wesley Publishing Company, 1998.

[6] DAY, I.J., "Stall Inception in Axial Compressors". Trans. ASME Journal of Turbomachinery, VOL. 155, pp. 1-9.

[7] DORCA, J.M.,"*Aplication of an Energy-Like Stability Metric for Axial Compressor Design*", Master's Thesis, Department of Aeronautics and Astronautics, Massachusetts Institute of Technology, 2003.

[8] FEULNER, M.R., "*Modeling and Control of Rotating Stall in High Speed Multi-Stage Axial Compressors*". Ph.D. thesis, Massachusetts Institute of Technology, 1994.

[9] FRÉCHETTE, L.G., "*Implications of Stability Modeling for High-Speed Axial Compressor Design*". Master's Thesis, Department of Aeronautics and Astronautics, Massachusetts Institute of Technology, Feb. 1997.

[10] GARZON, VICTOR E.; DARMOFAL, DAVID L., *"Impact of geometric variability on axial compressor performance"*. American Society of Mechanical

Engineers, International Gas Turbine Institute, Turbo Expo (Publication) IGTI, v 6 B, 2003, p 1199-1213

[11] GREITZER, E.M., WISLER, D.C.," *Gas Turbine Compressor Technology: Status and opportunities*", IGTIC 1999.

[12] GREITZER, E.M., "*Review – Axial Compressor Stall Phenomena*", Journal of Fluids Engineering (Jun. 1980), Vol. 102, pp. 134-168.

[13] GREITZER, E.M., "*Stability of Pumping Systems – The 1980 Freeman Scholar Lecture*", Journal of Fluids Engineering (Jun. 1981), Vol. 163, pp. 193-240.

[14] KERREBROCK, J.L., "*Aircraft Engines and Gas Turbines*", 2nd ed. The MIT Press, Cambridge, Massachusetts, 1992.

[15] LAMB, CAROLINE TWOMEY; DARMOFAL, DAVID L., "*Performance-based geometric tolerancing of compressor blades*". Proceedings of the ASME Turbo Expo 2004, v 5 A, 2004, p 203-210.

[16] LIEBLEIN, S., SCHWENK, F.C., BRODERICK, R.L., "*Diffusion Factor for Estimating Losses and Limiting Blade Loadings in Axial Flow Compressor Blade Elements*". NACA RM E53D01, 1953.

[17] LONGLEY, J., "*A Review of Nonsteady Flow Models for Compressor Stability*", ASME J. of Turbomachinery (Apr. 1994), pp. 202-215.

[18] MCDOUGALL, N.M., CUMPSTY, N.A., HYNES, T.P., *"Stall inception in axial compressors"*. Journal of Turbomachinery, VOL. 112 (1990), pp. 116-125.

[19] MOORE, F., AND GREITZER, E., "*A Theory of Post-Stall Transients in Axial Compressors: Part I – Development of the Equations*", ASME J. of Engineering for Gas Turbines and Power, Vol.108 (1986), pp. 68-76.

[20] PADUANO, JAMES D., E.M. GREITZER, A.H. EPSTEIN, "*Compression System Stability"*, Annual Rev. Fluid Mechs, 2001, 33:491-517.

[21] PERROT, V., "*A Design Optimization Framework for Enhanced Compressor Stability Using Dynamic System Modeling*", Master's Thesis, Department of Aeronautics and Astronautics, Massachusetts Institute of Technology, Aug. 2003.

[22] SIDWELL, VINCE; DARMOFAL, DAVID, *"A selective assembly method to reduce the impact of blade flow variability on turbine life Source"*, Proceedings of the ASME Turbo Expo 2004, v 5 A, 2004, p 267-276.

[23] SIEVERDING, F., CASEY, M., RIBI, B., MEYER, M., "*Design of Industrial Axial Compressor Blade Sections for Optimal Range and Performance*". GT2003-38036. In Proceedings of the ASME Turbo Expo 2003.

[24] SMITH, L.H., "*Compressor Aero Design at General Electric Before CFD*". Journal of Turbomachinery, Vol.124 (2002), pp. 321-330.

[25] SPAKOVSZKY, Z., "*Applications of Axial and Radial Compressor Dynamic System Modeling*", PhD Thesis, Department of Aeronautics and Astronautics, Massachusetts Institute of Technology, 2000.

[26] WECK, O., WILLCOX, K., "*Multidisciplinary System Design Optimization*", Class Notes, 16.888, MIT, Spring 2004.

[27] WEIGL, H.J., FRECHETTE, L.G., "*An Update on Compressible Stall Inception Modeling*". MIT Gas Turbine, Internal Document, 1997.

[28] YOUNGREN, H., DRELA, M., "*A User Guide to Mises 2.53*". MIT, Computational Aerospace Sciences Laboratory, December 1998.